

NAVAL POSTGRADUATE SCHOOL
Monterey, California



THESIS

**EVALUATION OF MICROSTRUCTURE OF
A 6092 Al - 17.5 VOLUME PERCENT SiC
PARTICLE REINFORCED COMPOSITE
USING ELECTRON BACKSCATTER
PATTERN (EBSP) ANALYSIS METHODS**

by

John J. Markovich

March 1998

Thesis Advisor:

Terry. R. McNelley

Approved for public release; distribution is unlimited.

19980512 046

DTIC QUALITY INSPECTED 3

REPORT DOCUMENTATION PAGE

Form Approved OMB No. 0704-0188

Public reporting burden for this collection of information is estimated to average 1 hour per response, including the time for reviewing instruction, searching existing data sources, gathering and maintaining the data needed, and completing and reviewing the collection of information. Send comments regarding this burden estimate or any other aspect of this collection of information, including suggestions for reducing this burden, to Washington Headquarters Services, Directorate for Information Operations and Reports, 1215 Jefferson Davis Highway, Suite 1204, Arlington, VA 22202-4302, and to the Office of Management and Budget, Paperwork Reduction Project (0704-0188) Washington DC 20503.

1. AGENCY USE ONLY (Leave blank)	2. REPORT DATE March 1998	3. REPORT TYPE AND DATES COVERED Master's Thesis	
4. TITLE AND SUBTITLE EVALUATION OF MICROSTRUCTURE OF A 6092 Al - 17.5 VOLUME PERCENT SiC PARTICLE REINFORCED COMPOSITE USING ELECTRON BACKSCATTER PATTERN (EBSP) ANALYSIS METHODS		5. FUNDING NUMBERS	
6. AUTHOR(S) John J. Markovich			
7. PERFORMING ORGANIZATION NAME(S) AND ADDRESS(ES) Naval Postgraduate School Monterey CA 93943-5000		8. PERFORMING ORGANIZATION REPORT NUMBER	
9. SPONSORING/MONITORING AGENCY NAME(S) AND ADDRESS(ES)		10. SPONSORING/MONITORING AGENCY REPORT NUMBER	
11. SUPPLEMENTARY NOTES The views expressed in this thesis are those of the author and do not reflect the official policy or position of the Department of Defense or the U.S. Government.			
12a. DISTRIBUTION/AVAILABILITY STATEMENT Approved for public release; distribution is unlimited.		12b. DISTRIBUTION CODE	
13. ABSTRACT (maximum 200 words) Microtexture and grain boundary misorientation data were obtained for a 6092 Al - 17.5 volume percent SiC particle-reinforced material as a function of processing history. Computer-aided electron backscatter pattern (EBSP) analysis methods in a scanning electron microscope were used to obtain grain-specific orientation measurements by traversing along a pattern of lines on the surface of a metallographic sample. As part of this project, it was necessary to develop ion milling methods to obtain a sufficiently strain free condition of the aluminum matrix to allow diffraction patterns to be obtained. These methods were applied to samples extruded at various strain rates and processing temperatures; the data revealed that recrystallization had occurred at all processing conditions. Analysis of crystal orientations and grain-to-grain misorientation data revealed random distributions consistent with predictions of the particle-stimulated nucleation theory of recrystallization. Additionally, spacing measurements were taken between orientation measurements. The result of this analysis indicated a very fine matrix microstructure.			
14. SUBJECT TERMS Discontinuous Reinforced Aluminum, Metal Matrix Composites, Matrix Microtexture, Electron Backscatter Pattern, Preferred Grain Orientation and Texture, Grain Misorientation, Recrystallization, Particle-Stimulated Nucleation		15. NUMBER OF PAGES 79	
		16. PRICE CODE	
17. SECURITY CLASSIFICATION OF REPORT Unclassified	18. SECURITY CLASSIFICATION OF THIS PAGE Unclassified	19. SECURITY CLASSIFICATION OF ABSTRACT Unclassified	20. LIMITATION OF ABSTRACT UL

Approved for public release; distribution is unlimited

**EVALUATION OF MICROSTRUCTURE OF A 6092 Al - 17.5
VOLUME PERCENT SiC PARTICLE REINFORCED COMPOSITE
USING ELECTRON BACKSCATTER PATTERN (EBSP) ANALYSIS
METHODS**

John J. Markovich
Major, United States Army
B.S., United States Military Academy, 1986

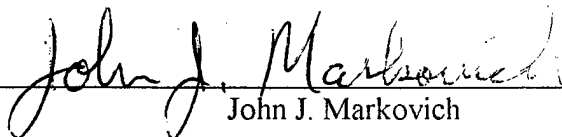
Submitted in partial fulfillment of the
requirements for the degree of

MASTER OF SCIENCE IN MECHANICAL ENGINEERING

from the

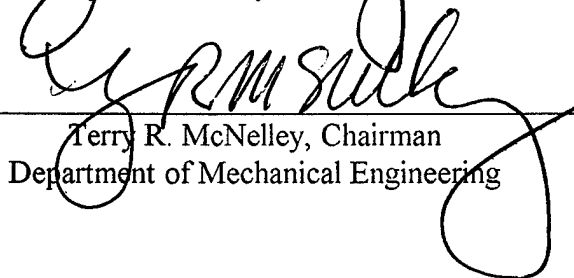
**NAVAL POSTGRADUATE SCHOOL
March 1998**

Author: _____


John J. Markovich

Approved by: _____


Terry R. McNelley, Thesis Advisor


Terry R. McNelley, Chairman
Department of Mechanical Engineering

ABSTRACT

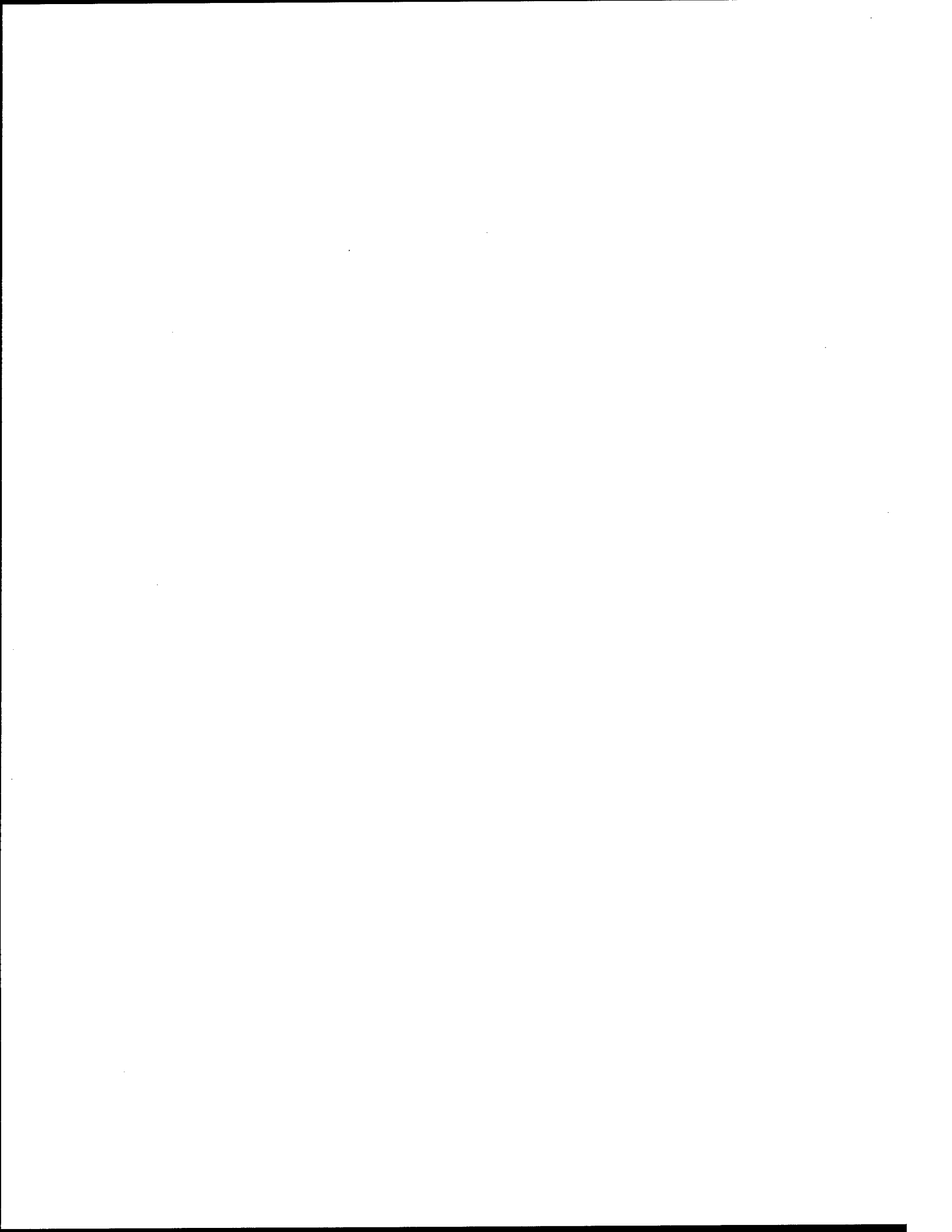
Microtexture and grain boundary misorientation data were obtained for a 6092 Al - 17.5 volume percent SiC particle-reinforced material as a function of processing history. Computer-aided electron backscatter pattern (EBSP) analysis methods in a scanning electron microscope were used to obtain grain-specific orientation measurements by traversing along a pattern of lines on the surface of a metallographic sample. As part of this project, it was necessary to develop ion milling methods to obtain a sufficiently strain free condition of the aluminum matrix to allow diffraction patterns to be obtained. These methods were applied to samples extruded at various strain rates and processing temperatures; the data revealed that recrystallization had occurred at all processing conditions. Analysis of crystal orientations and grain-to-grain misorientation data revealed random distributions consistent with predictions of the particle-stimulated nucleation theory of recrystallization. Additionally, spacing measurements were taken between orientation measurements. The result of this analysis indicated a very fine matrix microstructure.

TABLE OF CONTENTS

I.	INTRODUCTION.....	1
A.	COMPOSITE MATERIALS.....	1
B.	APPLICATION OF COMPOSITES.....	2
C.	THE NEED FOR DEVELOPING LIGHTER ARMOR WEAPONS PLATFORMS.....	3
D.	THE ROLE OF PROCESSING.....	4
II.	BACKGROUND.....	5
A.	MATERIAL	5
B.	DEFORMATION PROCESSING OF MMCS.....	5
C.	RECRYSTALLIZATION.....	6
D.	PARTICLE STIMULATED NUCLEATION.....	8
III.	EXPERIMENTAL METHOD.....	11
A.	MATERIAL SELECTION.....	11
B.	SAMPLE PREPARATION.....	13
C.	ION MILLING.....	14
D.	ANALYSIS BY ELECTRON BACKSCATTER DIFFRACTION.....	17
E.	GRAIN ORIENTATION ANALYSIS.....	22
F.	MEAN DISTANCE BETWEEN PATTERNS.....	25
G.	IMAGING.....	26
H.	CONTROL SAMPLE.....	27

IV.	RESULTS.....	29
A.	IMAGING.....	29
B.	MICROTEXTURE AND MISORIENTATION ANALYSIS.....	31
C.	MEAN DISTANCE BETWEEN PATTERNS.....	37
D.	UNREINFORCED 6061.....	38
V.	DISCUSSION.....	43
A.	COMPOSITE SAMPLE PREPARATION.....	43
B.	IMPLICATIONS OF THE TEXTURE AND MISORIENTATION DATA.....	43
C.	GRAIN SIZE.....	44
VI.	CONCLUSIONS AND RECOMMENDATIONS.....	49
A.	CONCLUSIONS.....	49
B.	RECOMMENDATIONS.....	49
	APPENDIX A. XRD ANALYSIS OF 13184.....	51
	APPENDIX B. SPACING MEASUREMENTS BETWEEN ELECTRON BACKSCATTER DIFFRACTION PATTERNS FOR 13183 MATERIAL.....	55
	APPENDIX C. SPACING MEASUREMENTS BETWEEN ELECTRON BACKSCATTER DIFFRACTION PATTERNS FOR 13185 MATERIAL.....	57
	APPENDIX D. SPACING MEASUREMENTS BETWEEN ELECTRON BACKSCATTER DIFFRACTION PATTERNS FOR 13186 MATERIAL (SiC PARTICLE LOCATIONS UNDERSCORED).....	59
	APPENDIX E. SPACING MEASUREMENTS BETWEEN ELECTRON BACKSCATTER DIFFRACTION PATTERNS FOR 13187 MATERIAL.....	61

LIST OF REFERENCES.....63
INITIAL DISTRIBUTION LIST.....67



I. INTRODUCTION

A. COMPOSITE MATERIALS

The field of composite materials has grown rapidly in the past two decades although some types of composites have been in use in engineering applications for much longer. Concrete reinforced with sand and polyester resin reinforced with glass fibers are two common examples of composites in wide use. A composite is a manufactured material consisting of two or more distinct phases which are distributed or arranged in three dimensions and with an interface separating them. It is characterized by property combinations better than those in any of the components by themselves [Ref. 1]. Composites can be further classified as continuous fiber, chopped whisker, or particulate materials according to the nature of reinforcement. Of these, particulate reinforced composites tend to have nearly isotropic properties while continuous fiber and whisker-reinforced materials are generally anisotropic.

Particulate reinforced metal matrix composites (MMCs) generally offer improved wear resistance, higher strength to weight ratio, and higher stiffness to weight ratio when compared with their unreinforced counterparts. As a subset of MMCs, discontinuous (particulate) reinforced aluminum (DRA) composites offer a significant increase in stiffness to weight ratios and extended wear resistance over their standard aluminum counterparts. They may also exhibit improved fatigue behavior as well. The most common DRAs are Al-Al₂O₃ (usually consolidated by melt processing techniques) and Al-SiC (usually consolidated by powder metallurgy methods). The research conducted in this study was concerned with an Al-SiC particulate composite formed by powder metallurgy methods.

B. APPLICATION OF COMPOSITES

Although not yet in widespread use, Al-SiC DRAs have been successfully used in specific high performance aircraft applications as a replacement material. One example is the ventral fin on the U.S. Air Force's F-16 aircraft. The higher stiffness and fatigue resistance of the Al-SiC composite fin provided an improved component life over the replaced monolithic aluminum alloy. The result was cost savings from increased life of the fin and increased safety margins for the aircraft. The material in this research was provided under a Title III program in conjunction with the Air Force via Wright Patterson Air Force Base.

For the U.S. Army, particular interest in DRA composites lies in lightweight armor applications. The opportunity exists to improve armor protection on combat vehicles, such as personnel carriers, without increasing the vehicle weight, or lowering the weight while maintaining the current level of aluminum armor protection. Also, as in the F-16 example, extending the life of other ground vehicle components could result in substantial cost savings when applied across an entire fleet of tactical trucks.

DRAs have shown superior ballistic performance over standard aluminum alloys in testing [Ref. 2]. Recently, it has been suggested that the development of functionally graded composite materials may offer even greater improvements in ballistic protection. The concept is that a gradient in volume fraction of particles in the matrix, as well as particle size, with a greater concentration of particles toward the outer surface, will result in improved shock wave attenuation (and hence reduced spall effect), provide a harder front face to projectiles, and offer better resistance to crack propagation in mid and back face regions when processed for adequate toughness [Ref. 3].

C. THE NEED FOR DEVELOPING LIGHTER ARMOR WEAPONS PLATFORMS

In the Cold War, the principal focus of military weapons platform designers was the Soviet threat in the Central European theater. To overcome the superior numbers of Warsaw Pact tanks, NATO and American armor was designed to exceed the corresponding performance parameters of Soviet equipment in both armor protection and armament. Maximizing the performance parameters led directly to increased vehicle weight. The Army's main battle tank, the M1A1 Abrams, weighs in excess of 65 tons when combat loaded. Indeed, it proved to be a superior tank in the Gulf War when pitted against Soviet made equipment. But with the fall of the Soviet Union, the strategic situation has changed. To meet the new strategic needs of the country, the Army has deployed more frequently but in smaller numbers to more diverse locations. Bosnia/Herzegovina, Rwanda, Haiti, and Somalia are the most recent examples. Rapid deployability of forces, including armored vehicles, is essential to success in these situations. However, the time required to deploy a 65 ton vehicle to a remote location makes its use unlikely in short notice operations. Their sheer weight makes their mobility very low, especially in some third world countries where roads and bridges are not designed to carry such weight. These issues severely limit both the amount and manner in which armored vehicles have been used in these recent deployments. The development and use of DRAs in armor applications could help to usher in a generation of improved, light weight armor vehicles that are better suited for rapid deployment to remote areas in the world while providing a high level of armor protection.

D. THE ROLE OF PROCESSING

Processing has proven to be the key in maximizing the properties in DRAs. But a lack of understanding the full relationship between processing and mechanical properties has hindered the choice of these materials in many potential applications. Typically, the main drawback to using DRAs has been relatively poor ductility as well as fracture toughness. Recently, work in this laboratory has shown that DRAs can be processed to obtain fracture toughness/strength combinations comparable to standard aluminum alloys that correspond closely to the composite matrix.

In predicting the microstructure associated with processing DRAs, Humphreys' theory of particle stimulated nucleation (PSN) of recrystallization has been used with some success [Ref. 4,5], but there has been little work on matrix microstructures obtained for a wide range of composite processing conditions. Transmission electron microscopy (TEM) has been done [Ref. 6], but is subject to sample size/area limitations.

The object of this research, therefore, is to further the understanding of these composites by defining the matrix microstructure after extensive processing by application of newly developed computer aided electron backscatter pattern (EBSP) analysis methods.

II. BACKGROUND

A. MATERIAL

As discussed in the introduction, the two most common reinforcing particles employed in DRAs are silicon carbide (SiC) and alumina (Al_2O_3). There are cost trade-offs in choosing between the two classes of DRA materials. Alumina can be introduced to an aluminum alloy matrix by melt processing. Silicon carbide requires powder metallurgy (PM) because it is reactive with molten aluminum. Composites containing SiC apparently offer better mechanical properties and may require less post-consolidation processing to complete the redistribution of reinforcing particles. This fact may make the SiC reinforced composite a better choice in terms of life cycle costs for applications requiring superior properties even though it is a more expensive material in terms of cost per unit weight in the consolidation phase. In turn, this may make the SiC particulate composite potentially more attractive to the Defense Department in an era of declining budgets.

B. DEFORMATION PROCESSING OF MMCs

In both fabrication methods some particle clustering occurs and post-consolidation processing involving true strains upwards of 4.0 is required to get a uniform distribution of particles [Ref. 4,5,7-10]. Here, the material was provided in the form of extrusions.

Prior work done at the Naval Postgraduate School on DRAs has indicated that the PSN model can correctly predict the microstructures obtained in DRAs containing Al_2O_3 and processed to large strains. Included in the model is the effect on recrystallized matrix grain size of both particle size and volume fraction of the reinforcement [Ref. 4,5,7-12]. However, the mechanism by which the particles become uniformly distributed during deformation processing is an important remaining question; recrystallization may have a role in particle redistribution but the details remain to be resolved.

Work in this laboratory has also studied the effect of processing on fracture properties of DRAs. Prior processing has been shown to have an effect on the fracture toughness/strength relationship. The materials can be processed to produce grain refinement which results in toughness/strength combinations exceeding that of unreinforced 6061 Al. These effects have been attributed, at least in part, to processing conditions. [Ref. 6]

C. RECRYSTALLIZATION

Recrystallization generally refers to the replacement of deformed grains by new, strain free grains. Strain energy due to deformation is stored primarily in the form of dislocation structures. Dislocation rearrangement within such structures may take place and this is known as recovery [Ref. 13,14]. High-angle grain boundaries may also form although the details have yet to be established on precisely how this occurs within the deformation microstructure. Once high-angle boundaries have formed, recrystallization becomes the process of high-angle boundary migration into surrounding regions (where

the newly-formed, high-angle boundaries enclose strain free material) until the new grains impinge and the material then becomes completely softened.

In order for recrystallization to occur it is necessary that local lattice reorientation develops during plastic deformation. This localized reorientation, or curvature, results from the build up and storage of dislocations which usually are distributed in some form of non-uniform cellular arrays. Dislocation build up and the development of local lattice curvature may occur readily during low-temperature deformation. A cold deformed material usually must be heated in order to induce recrystallization since the formation of high-angle boundaries apparently requires energy to complete the rearrangement within the cellular deformation structure. Both lattice reorientation and high-angle boundary formation can occur during deformation at intermediate temperatures so recrystallization can take place in conjunction with plastic deformation. At high deformation temperatures recovery may become so rapid that no lattice curvature develops, and then recrystallization can not occur.

In DRAs, the plastic accommodation of large ceramic particles may result in localized lattice reorientation during plastic deformation. Therefore the particles themselves may become initiation sites for recrystallization. This has been considered in the development of the particle stimulated nucleation (PSN) theory by Humphreys [Ref. 11,12]. Work in this laboratory has indicated that the redistribution of particles during deformation processing occurs more readily during elevated temperature deformation when PSN occurs. Relative displacement of particles within clusters may occur more readily as recrystallization facilitates grain boundary sliding within particle clusters.

D. PARTICLE STIMULATED NUCLEATION

PSN requires that enough energy be stored in the deformation zone within the matrix around the particles to allow recrystallized nuclei to grow away from the particles. The large strains associated with the extrusion of the DRA materials are generally sufficient to generate the requisite dislocation structures around the particles. Recrystallization may then occur at these nucleation sites [Ref. 11-13]. If one grain forms at each particle, the expression [Ref. 12] which describes the grain size is

$$D_{PSN} = \frac{d_p}{f_v^{1/3}} \quad (1)$$

where D_{PSN} is the recrystallized grain size, d_p is the particle size and f_v is the volume fraction of reinforcing particles.

Deformation processing by extrusion of the material is always done at elevated temperatures. Above a certain critical temperature, recovery by dislocation climb will occur and preclude development of lattice curvature in the deformation zones around particles [Ref. 12]. Thus a critical deformation strain rate is required in order for deformation zones to form during elevated temperature straining. This critical rate is given by the expression [Ref. 12]:

$$\dot{\varepsilon}_c = \frac{K_1}{T d_p^2} \exp\left(-\frac{Q_v}{RT}\right) + \frac{K_2}{T d_p^3} \exp\left(-\frac{Q_b}{RT}\right) \quad (2)$$

where K_1 and K_2 are constants, R is the universal gas constant, T is absolute temperature, Q_v is activation energy for volume diffusion, and Q_b is the particle/matrix interface

diffusion activation energy. Previous work by Humphreys and Kalu [Ref. 12] has suggested that the second term dominates the expression such that

$$\dot{\epsilon}_c \cong \frac{K_2}{Td_p^3} \exp\left(-\frac{Q_b}{RT}\right) \quad (3)$$

and thus describes the processing conditions for initiating PSN in Al-Si and Al-Ni materials. Applying the values of K_2 and Q_b given by Humphreys and Kalu, the critical strain rate was calculated by Hoyt [Ref. 4] and is plotted as a function of processing temperature and particle size in Figure 2.1.

For a given particle size, the data in Figure 2.1 may be used to estimate the processing temperature and strain rate for PSN. Above the curve, recovery results in relaxed dislocation structures, and PSN is not expected. Conversely, below the curve, the

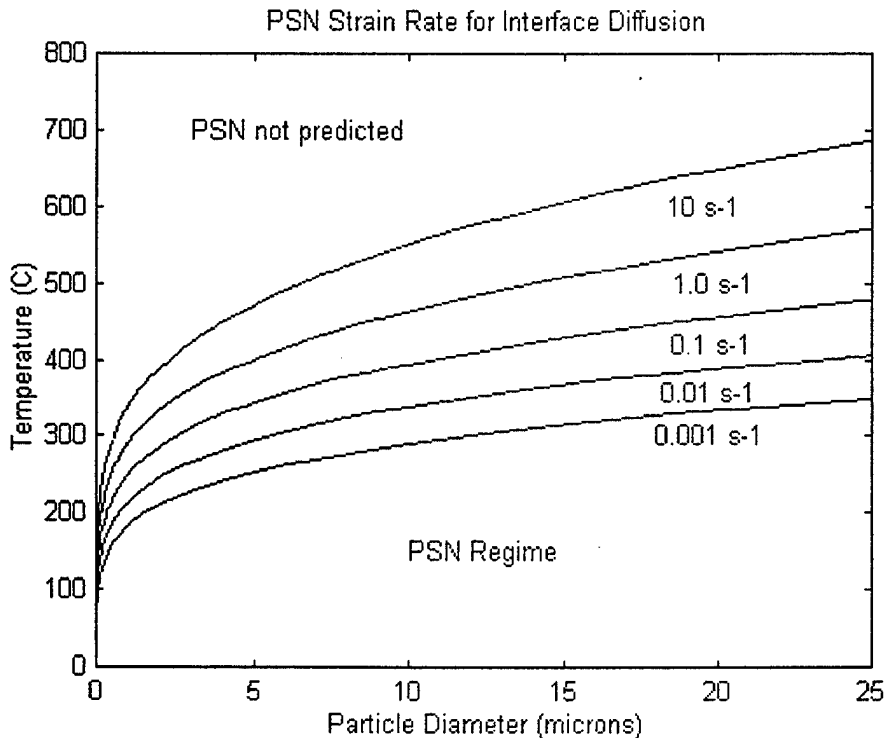


Figure 2.1. PSN Critical Strain Rate. From Ref. [4].

particles are expected to become nucleation sites.

By selecting materials processed with various different conditions in accordance with the plot in Figure 2.1, we can investigate further the extent of PSN at each processing condition and thereby to define the matrix microstructure in the DRA. Analyzing texture, misorientation data, and grain size from samples processed within, outside, and at the predicted PSN condition will help us to better understand the application of the Humphreys model to this particular DRA.

III. EXPERIMENTAL METHOD

A. MATERIAL SELECTION

The DRA material selected for this particular experimental investigation was a powder metallurgically processed 6092 Al (with an initial Al powder particle size of 30-50 μm) reinforced with 17.5 volume percent SiC particles (with a mean particle size of 7 μm). The material was consolidated in the form of a 19in. diameter billet and extruded at 500° C to a true strain of 3.38, producing a billet of 3.5in. in diameter by DWA Composites of Chatsworth, California, USA. The billet was trimmed to a diameter of 3in. and extruded through streamlined dies under four different conditions to produce bars with rectangular cross sections of 1.484 x 0.484in., for a total true strain of 5.67 following powder consolidation. Elemental composition of the Al alloy is given in Table 3.1. [Ref. 6]

<u>Element</u>	<u>Weight %</u>
Silicon	0.40 - 0.80
Magnesium	0.80 - 1.20
Copper	0.70 - 1.00
Manganese	0.15 max.
Chromium	0.15 max.
Zinc	0.25 max.
Titanium	0.15 max.
Iron	0.70 max.
Oxygen	0.05 - 0.50
Others, each	0.05 max.
Others, total	0.15 max.
Aluminum	Remainder

Table 3.1. Chemical analysis of 6092 Al with 17.5% SiC. From Ref. [19].

The second extrusion was done at the Air Force Materials Laboratory at Wright Patterson Air Force Base, Ohio. The selection of processing strain rates and temperatures for this latter series of extrusions was based on Hoyt's [Ref. 4] analysis (discussed in Chapter II), such that some of the material would be processed well into the predicted PSN regime, some at the predicted critical temperature, and, finally, some into the area where no PSN is expected to occur (Figure 3.1). The processing conditions for each material are listed in Table 3.2.

Designation	Predicted Regime	Strain Rate (s^{-1})	Extrusion Temp. ($^{\circ}C$)
13183	PSN	6.0	350
13184	Intermediate (PSN)	6.0	450
13185	Intermediate (PSN)	6.0	400
13186	Intermediate (Non-PSN)	0.6	400
13187	Non-PSN	0.6	500

Table 3.2. Processing conditions for the various samples studied.

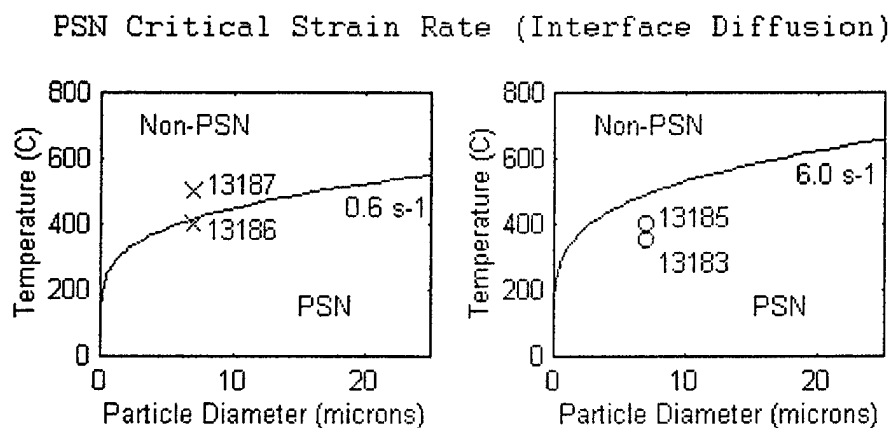


Figure 3.1. Material processing conditions selected in accordance with Equation (3).

B. SAMPLE PREPARATION

The as-extruded bars were sectioned to provide wafers with planes corresponding either to the NP plane or the TP plane (Figure 3.2). These were cut with a Buehler diamond saw to approximately 1mm thickness. The wafers were then mounted to an aluminum sanding block with hot wax. Care was taken to heat the wax to the minimum temperature necessary to melt the wax for mounting. Once the wafer was mounted on the block, it was cooled with an air gun to minimize the temperature effect on the sample. It was typically back to room temperature in about 10 minutes.

After allowing the wax mounting to set (minimum time of one hour), the sample was ready to be polished. The polishing consisted of wet polishing on progressively finer grits on a schedule repeating the work of Quiles [Ref. 15], with minor variations at the end of the process in the diamond paste polishing steps. The technique is outlined in Table 3.3.

Once the sample was mechanically polished, a 3mm disk was cut out of the wafer. Disks were punched out with a sample punch when the wafers sufficiently thin. For samples of thickness in excess of about $40\mu\text{m}$, the punch is inadequate. Disks were cut out of these with an electric discharge machine (EDM). Mechanical polishing induces strain at the surface of the sample and precludes the formation of diffraction patterns required for diffraction analysis in the SEM. Electron backscatter patterns are formed in a layer on the order of 30nm in depth. Chemical and electropolishing methods are often used on Al alloys but have not worked for SiC reinforced Al alloys. This is because both methods tend to preferentially attack the particle/matrix interface rather than the matrix

grain boundaries. However, some consistent success has been achieved on TEM samples with ion milling [Ref. 6].

Step no.	Polishing Medium	Grit size	Grit Diameter (microns)	Time (min)	Wheel (RPM)	Comments
1	Carbide Paper	320	46	0.5	12" dia/ 300rpm	1-5 lbf
2	Carbide Paper	500	30	0.5	12" dia/ 300rpm	1-3 lbf
3	Carbide Paper	1000	18	2.0	12" dia/ 300rpm	1-3 lbf
4	Carbide Paper	2400	10	3.0	12" dia/ 300rpm	1-3 lbf
5	Carbide Paper	4000	5	3.0	12" dia/ 300rpm	1-3 lbf
6	Diamond Spray w/ Metadi Chemnet Cloth		6	3.0	12" dia/ 250rpm	1 lbf
7	Diamond Spray w/ Metadi Chemnet Cloth		1	1.5	12" dia/ 250rpm	1 lbf

Table 3.3. Mechanical polishing technique. After Ref. [15].

C. ION MILLING

Analyzing the matrix microstructure to investigate PSN effects is a difficult task. The lack of published micrographs attests to the inherent difficulty in sample preparation for this. Micrographs of these composites are often used to show particle distribution and orientation. But the ability to view the grain boundary or to obtain orientation contrast in the matrix is severely limited by the presence of the reinforcing particles.

Processing samples by ion milling is a technique common in preparing TEM samples. The ion milling apparatus bombards a 3mm diameter sample with an inert argon plasma (Figure 3.3) in which ions and electrons are accelerated through a 5kV potential, thus sputtering material off of the surface of the sample [Ref. 16]. This is done to both sides of the sample in order to thin a TEM sample. Thinning TEM samples of Al-SiC composite samples by ion milling left the sample sufficiently strain free to view microstructure and to obtain diffraction patterns [e.g. Ref. 6]. Therefore, it was postulated that ion milling might be an acceptable method of preparing SEM samples for EBSP analysis.

A shallow angle of 10 degrees was used to limit surface deformation due to ion implantation, and only the top ion gun was used since only the strained outer layer of the sample surface was to be sputtered away. Removing several atomic layers in order to look at a nearly strain free aluminum matrix is necessary to analyze the microstructure using the electron backscatter diffraction patterns.

The samples in this experiment were milled at room temperature rather than at reduced temperatures. Cold milling with liquid nitrogen is normally useful as it makes the surface of the sample more brittle and helps prevent re-implantation of sputtered sample material [Ref. 16]. However in this Al-SiC composite, the difference in thermal expansion coefficients would cause the aluminum to contract more than the SiC resulting in additional straining of the Al matrix. Finally, the goal in milling was to get as flat a surface as possible in addition to a strain free condition.

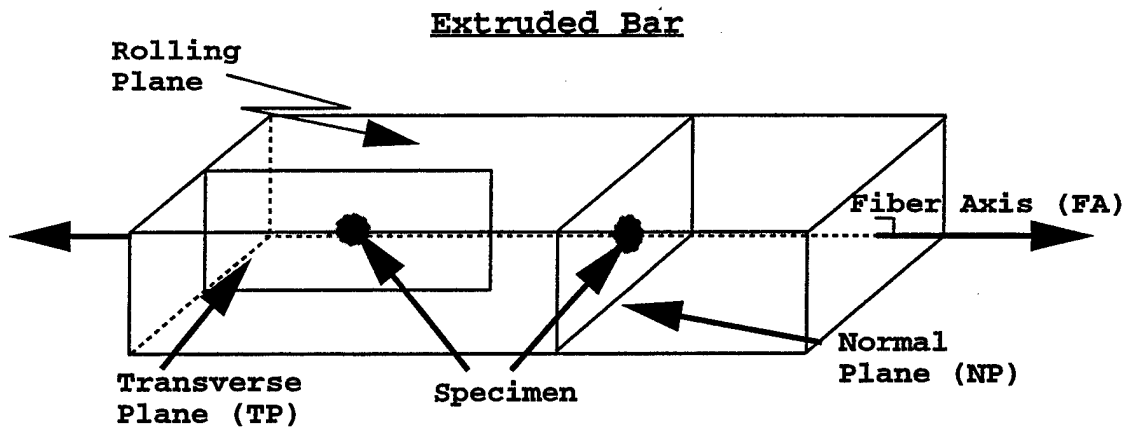


Figure 3.2. Schematic of extruded bar.

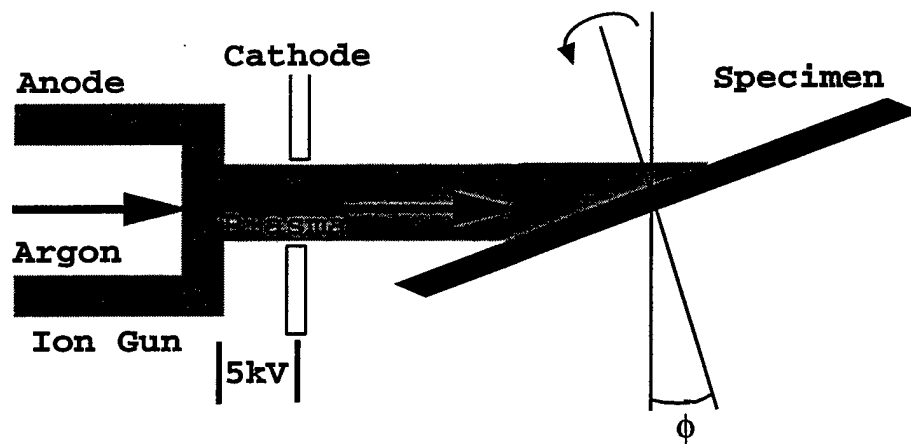


Figure 3.3. Schematic of Ion Miller. With Ref. [16].

A trial and error method determined that the optimum time for the sample to be in the ion mill was 15 hours. This period of time provided samples giving the best diffraction patterns without causing excessive surface roughness. Ion milling, however, does result in significant surface roughness (Figure 3.4 and 3.5). One additional sample was chemically polished with colloidal silica prior to ion milling in an effort to improve further the flatness of the sample prior to going into the ion mill. Although that treatment appeared to assist in the optical microscopy, the surface was just as rough as those samples not chemically polished. Ion milling, as noted above, did provide a sufficiently strain free surface for analysis by EBSD methods.

D. ANALYSIS BY BACKSCATTER ELECTRON DIFFRACTION

Diffraction of an electron beam occurs when the Bragg condition is met for elastic scattering of electrons. The beam has to interact with a periodic arrangement of atoms (as in a crystal structure) such that

$$n\lambda = 2d \sin \theta \quad (4)$$

where n is the order of diffraction, λ is the wavelength of the electrons, d is the interplanar spacing, and θ is the diffraction angle. Diffraction patterns, similar to Kikuchi patterns, but known as electron backscatter patterns result from diffraction of a divergent source of electrons generated within the sample just beneath the point where the primary electron beam strikes the specimen (Figure 3.6). The electrons that contribute to the pattern are only those that have lost no more than a few electron volts of energy and emerge from a depth in the specimen of no more than 30 to 40 nm. [Ref. 17]

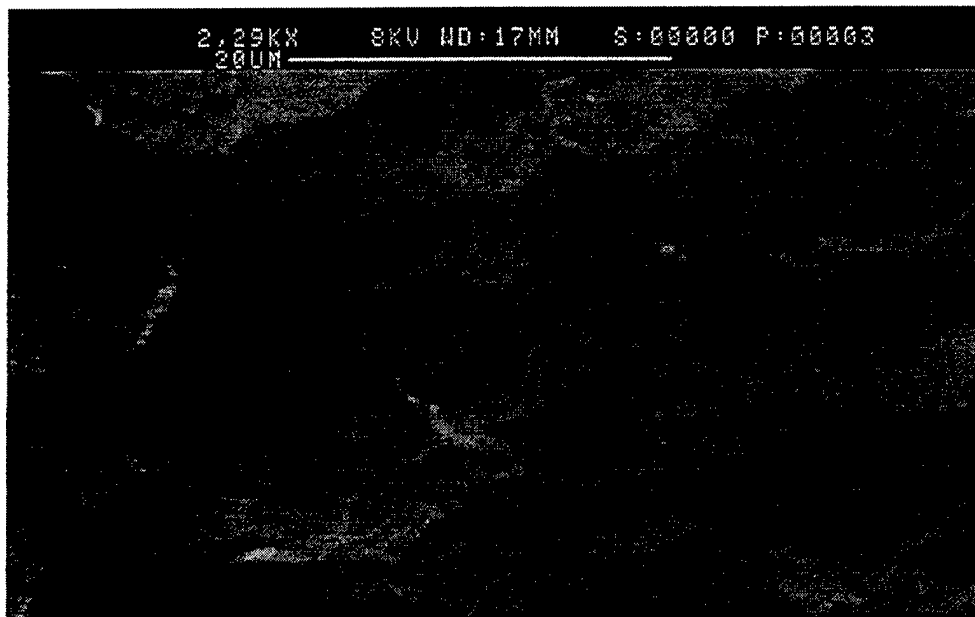


Figure 3.4. Secondary image of 13185 sample, transverse plane, with LaB₆ beam source. Note the surface roughness caused by ion milling (no etchant).

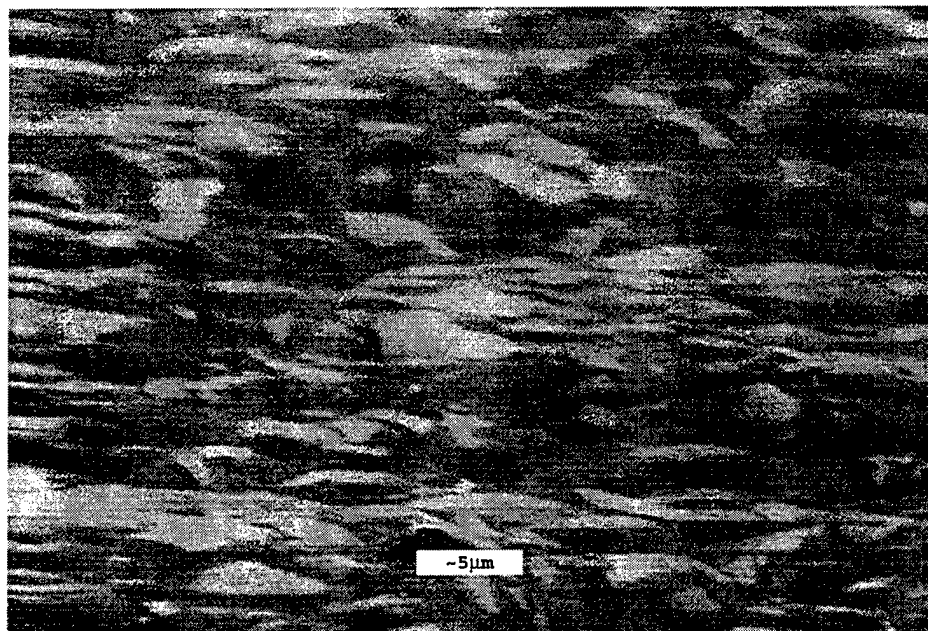


Figure 3.5. Surface roughness shown after ion milling of sample 13184, normal plane, 6kV, W source, 70 degree tilt, BSE image. Note surface roughness (no etchant).

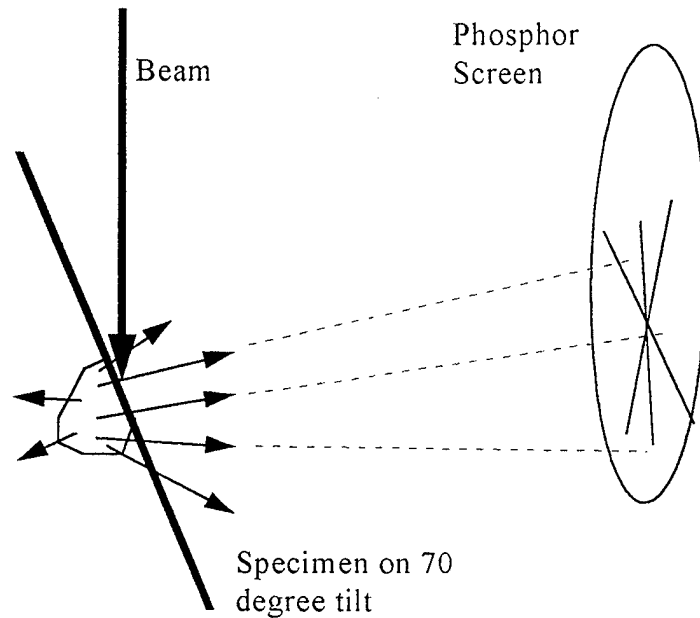


Figure 3.6. Schematic of formation of EBSP.

The orientation of the crystal can be determined by analyzing the various poles represented in the pattern. The electron beam is sufficiently small that individual grain orientations can be obtained. With each grain having its own specific orientation (Figure 3.7), a series of diffraction patterns can be observed and analyzed in relation to each other by noting reorientation of the diffraction pattern as successive orientations are displayed. The orientation of the crystal lattice is measured with respect to a set of default axes in terms of Euler rotation angles. This is the essential aspect of the EBSP method of analyzing texture and misorientation data with the automated pattern recognition (APR) program developed by TEXSEM Laboratories. Grain-to-grain misorientation information can be obtained by calculating the reorientation necessary to transform one orientation

into the adjacent orientation through matrix calculations based on the Euler angles [Ref. 17].

Diffraction patterns are acquired by a low-light camera focused on a phosphor screen inside the SEM chamber (Figure 3.8). The camera signal is sent to a television monitor. The camera control unit then integrates, freezes, and subtracts background interference prior to transmitting the pattern onward for computer analysis. The software package captures the diffraction pattern, analyzes it, and assigns Euler angle values. As this is done over a series of patterns, a data file is compiled. After a sufficient quantity of data points is collected, a series of rotations are applied to the data, depending on the plane examined (TP, RP, or NP see Figure 3.2) and the direction of the Fiber Axis (FA) of the sample relative to the default set of axes assumed by the APR program. To increase the signal-to-noise ratio of the pattern, the sample is placed in a holder inclined at 70 degrees and facing the phosphor screen (Figure 3.8).

Adopting this method to analyzing DRA composites requires the ability to recognize the difference between the diffraction pattern generated by the Al alloy matrix and that of the SiC particles. While traversing the spot to generate diffraction patterns, there is no image of the sample and the operator cannot 'see' the SiC particles.

Collecting data from Al matrix grains that cannot be discerned by standard SEM and optical techniques is the benefit of using this technique. Information on the grain orientation, or texture, and grain misorientation was acquired and analyzed. A technique (Figure 3.7) analogous to a mean linear intercept measurement of grain size was used so careful accounting of the distance from diffraction pattern to diffraction pattern

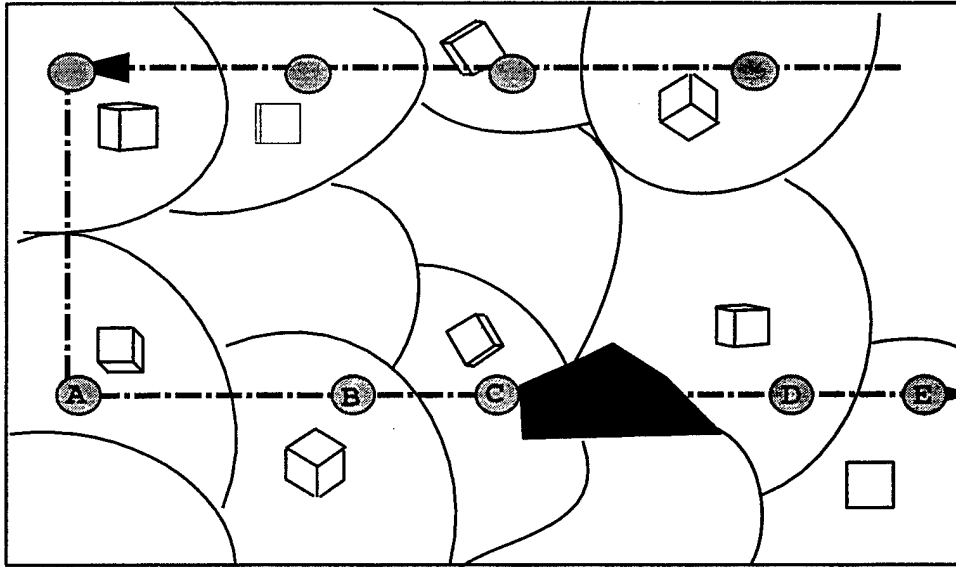


Figure 3.7. Representation of crystallographic grain orientation. With Ref. [17].

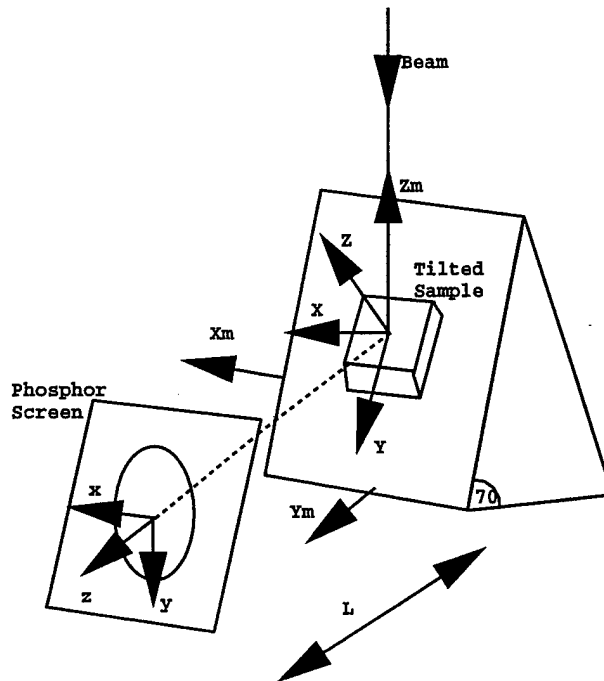


Figure 3.8. Schematic of projected diffraction pattern from sample at 70 degree tilt with respect to incident electron beam. From Ref. [18].

was made in order to reveal information on grain size as well.

E. GRAIN ORIENTATION ANALYSIS

Once the disk had been milled for 15 hours, it was placed in the 70° tilted holder and set in the SEM chamber with the holder facing toward the phosphor screen. In SE mode, the magnification was set at 2500x and the image was properly focused. While in this mode the background scattering was collected by the camera control unit for subtraction when collecting images in the spot mode. The spot size was set at 12 for the TOPCON 510 SEM, which equates to a probe diameter of about 110nm. This was the minimum spot size for which patterns can be acquired. It must be checked later with grain size determination. An oversized spot pattern will give erroneous results as it approaches the actual grain size itself.

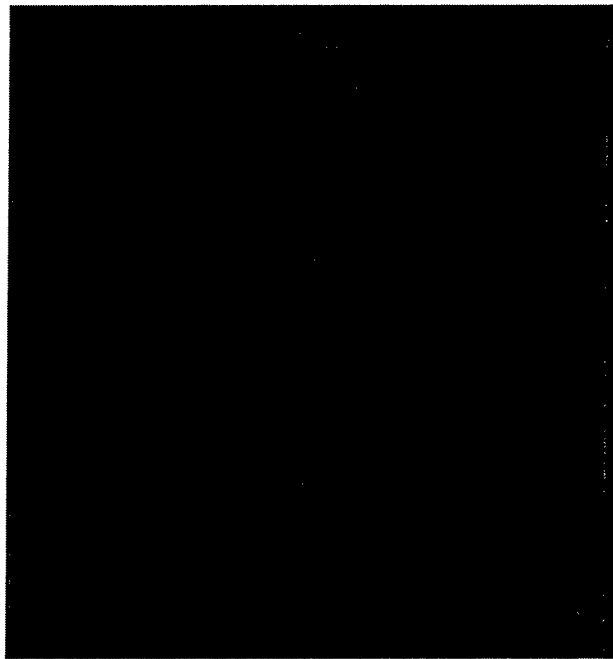
The recommended acceleration voltage for the beam is 20kV. At 70° tilt, the shallowness of the angle limits absorption and maximizes the signal sent to the camera. Only 30nm of the surface is involved in the determination of the crystal orientation [Ref. 17].

While traversing the spot, a pattern of lines appears on the screen indicating a diffraction pattern. Upon command, the camera control unit integrates a preset number of frames (16 in this case) and subtracts the background scattering. The pattern is then captured by the APR software for analysis. By analyzing a digitized version of the captured image for line width, line intensity, and the angular relationships between the various diffraction lines, a pattern is indexed to match the diffraction pattern seen on the

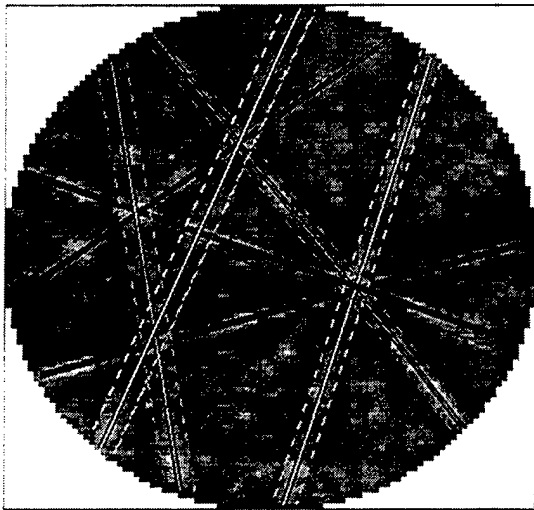
screen. (The software was also preset for the cubic symmetry of fcc Al.) Information from this pattern index is then written to a file maintaining data on each successive indexed pattern. Each pattern data line includes three Euler angles ϕ_1 , Φ , and ϕ_2 , an image quality index, and the name of the pattern (typically a number in succession). The Euler angles are angles referencing the orientation of the pattern in regards to an arbitrary orientation. This arbitrary orientation is usually a set of axes related to the sample's geometry, e.g. the fiber axis, etc. The default set of axes in the APR program assumes the rolling direction is up and down, the transverse direction is left to right, and the normal direction is normal to the surface of the specimen (Figure 3.8). The image quality index is a measure of the difference in contrasts between the pattern lines which are bright, and the spaces between the lines which are dark. Figure 3.9 shows the images seen associated with these steps.

Operator training was necessary to obtain familiarization on diffraction patterns generated by SiC particles. The SiC in this material is hexagonal and so a diffraction pattern with 6 fold symmetry is generated. The pattern generated for the $\langle 110 \rangle$ pole of the Al matrix looks similar, but does not, in fact, have this same symmetry. The crystal structure of the SiC particles was confirmed to be hexagonal with an x-ray diffraction (XRD) analysis on a separate sample (Appendix A).

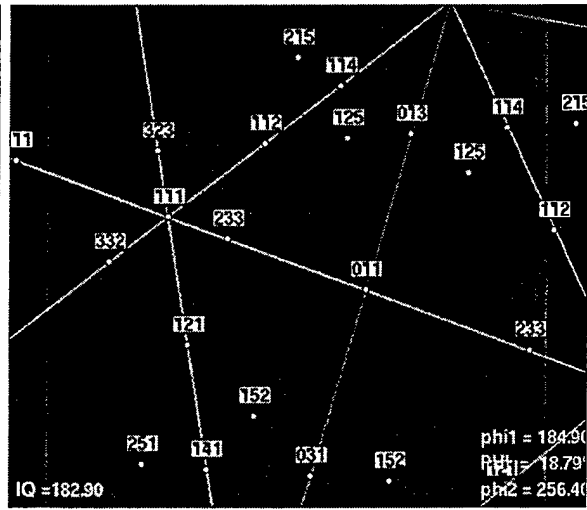
Three hundred data points were collected from each sample, except for the 13186 sample for which 400 data points were collected. Figure 3.7 shows a schematic of this technique of traversing the spot to collect EBSP data. Once the requisite number of data points had been collected, the orientation data of all the patterns can be analyzed by



(a)



(b)



(c)

Figure 3.9. The three steps in the automatic pattern recognition process: (a) acquire the pattern, (b) let the program analyze the pattern, and (c) confirm the pattern and store the data. From Ref. [19].

the software. A series of rotations must first be applied to the data. The APR program version 1.5 assumes a default orientation based on the geometry of a rolled plate where the rolling direction is up-down, the transverse direction is left-right, and the normal direction comes out of the paper. Since these samples were placed in the holder with the fiber axis (FA) oriented left-right, a 90 degree rotation is required to align the data in the pole diagram with the standard default axes. Additionally, a 45 degree rotation is required in APR 1.5 to account for beam geometry. Subsequent versions of the software have been corrected for this latter rotation [Ref. 19].

The misorientation histogram was then plotted comparing the orientation of one grain's pattern with the next. A histogram shows the frequency of boundaries by 5 degree increments. The samples from the PSN regime were expected to show a preponderance of high-angle grain boundaries while the samples from the non-PSN regime were expected to show more low-angle boundaries, reflecting a predominance of recovery effects.

F. MEAN DISTANCE BETWEEN PATTERNS

In an attempt to determine the grain size, a procedure analogous to the mean linear intercept (MLI) method described in the Metals Handbook [Ref. 20] was developed. However, instead of measuring distances between successive boundaries on a micrograph, measurements instead were recorded on the distance between successive grains based on distance between successive points where diffraction patterns were obtained. Supposing that the clearest pattern observed was at or near the center of the grain, an estimate could

be made of the mean distance between patterns (MDP), based on the MLI formula for particulate structures:

$$\lambda = \frac{1 - (V_v)_\alpha}{N_L} \quad (5)$$

where λ is the mean edge-to-edge distance, V_v is the volume fraction of α particles, and N_L is the number of particle interceptions per unit length of test line [Ref. 20].

Distances were measured as the spot is traversed from one diffraction pattern to the next. A template was made for the x and y traversing knobs of the microscope based on the magnification selected. This was necessary since the microscope does not have a readout indicating the distance traversed by the spot. The patterns were then logged by hand as the data points were collected. Equation (5) accounts for the distance between two successive patterns which are astride a SiC particle (Figure 3.10). This is a first attempt to determine the grain size of the Al matrix and the influence of processing history on this important microstructural parameter. Possible sources of error for this technique are described later in Chapter V.

G. IMAGING

A limited amount of imaging was done with both LaB₆ and W filaments as the electron beam source. The tungsten provides greater image stability while the LaB₆ provides a more coherent source and a brighter picture at smaller spot sizes. At normal accelerating voltages (e.g. 20kV) and in the secondary electron (SE) imaging mode, the depth of beam penetration makes for very incoherent pictures due to atomic number (or Z)

contrast. There is contrast from both the particles on the surface and those just beneath the surface.

Reducing the accelerating voltage and switching to the back scatter electron (BSE) imaging mode helps to alleviate this. At around 5kV, the distinction between aluminum and SiC on the surface becomes clear. Orientation contrast, and hence grain size information, is also more likely to be observed in this range. However, the low accelerating voltages while using BSE provide only a limited focus, however, due to the low energy associated back scattered electrons.

H. CONTROL SAMPLE

As a control sample, a rolled 6061T6 Al sample was used in an attempt to confirm the analysis technique used. As a monolithic alloy, it has a well documented texture [Ref. 21]. A TP oriented sample was cut from the 6061T6 material. It was polished with 1000 grit, 2400 grit, and 4000 grit SiC paper for 30-45 seconds each prior to electropolishing. The electropolishing was conducted in a 30% nitric 70% methanol solution for 30 seconds at -20°C and 7 volts and 0.5 amps. It was then placed in the 70 degree holder and 300 EBSP data points were collected. The operating conditions were: accelerating voltage of 20kV, magnification of 250x, and the spot size was 12 (approximately 110 nm by TOPCON literature).

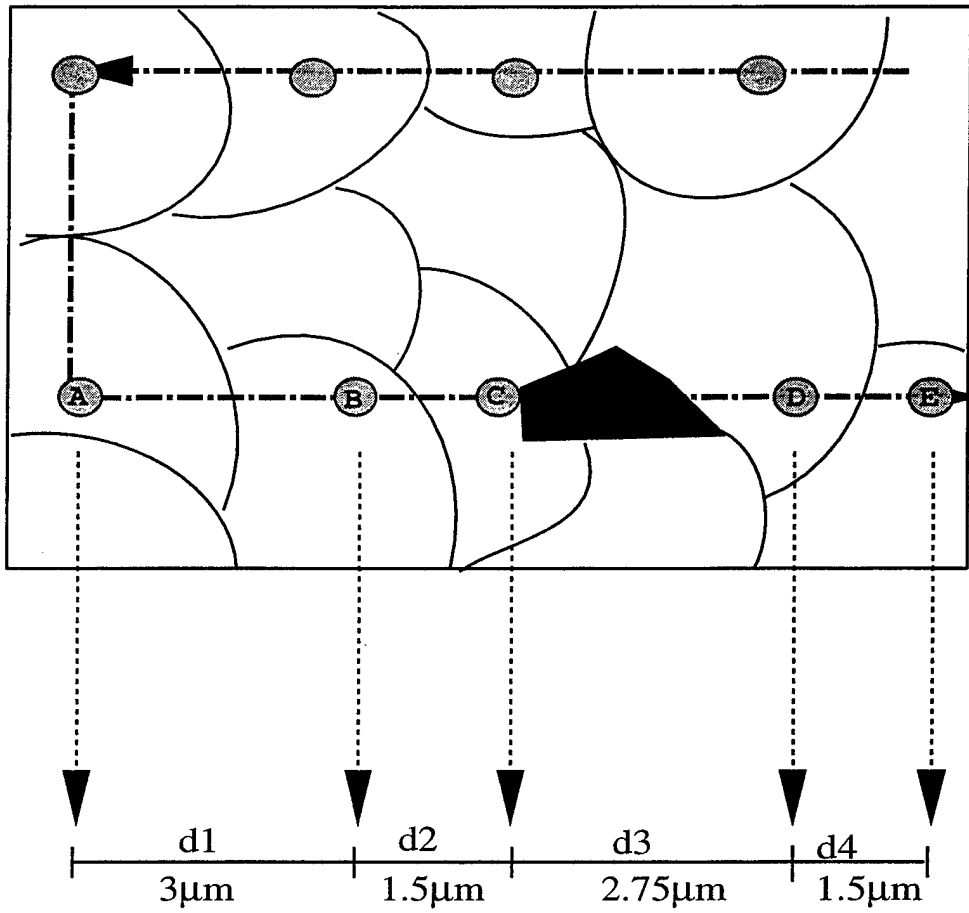


Figure 3.10. Schematic of MDP determination. Overhead view of beam traversing path with distances between diffraction patterns displayed.

IV. RESULTS

The research conducted in this experiment provided distinct results in the areas of imaging, microtexture, boundary misorientation, and separation distance between successive patterns. Each provides a part of the overall information sought about the matrix microstructure of this DRA and together the results provide insight into microstructural transformations during deformation processing.

A. IMAGING

While backscatter electron imaging has been successfully applied in examination of microstructure in Al alloys, low accelerating voltages ($\sim 5\text{-}6\text{kV}$) are required in multiphase materials. At higher accelerating voltages, atomic number contrast is very high and it is not possible to resolve contrast variation due to orientation effects, in the matrix. But at low accelerating voltages focus is inherently degraded.

The backscatter image in Figure 4.1 shows atomic number contrast (dark areas are lower in average atomic number), which reveals both SiC particles, and orientation contrast in the Al alloy matrix. The angular matrix features are grains or subgrains. Note in Figure 4.2 that such contrast is distinct from the roughness produced from the ion milling. The contrast data suggest the presence of a grain/subgrain structure on the order of $2.5\mu\text{m}$ in size in 13184 ($\dot{\epsilon} = 6\text{s}^{-1}$, $T = 450^{\circ}\text{C}$). The micrograph in Figure 4.1 represents the best image quality achieved thus far with this technique.

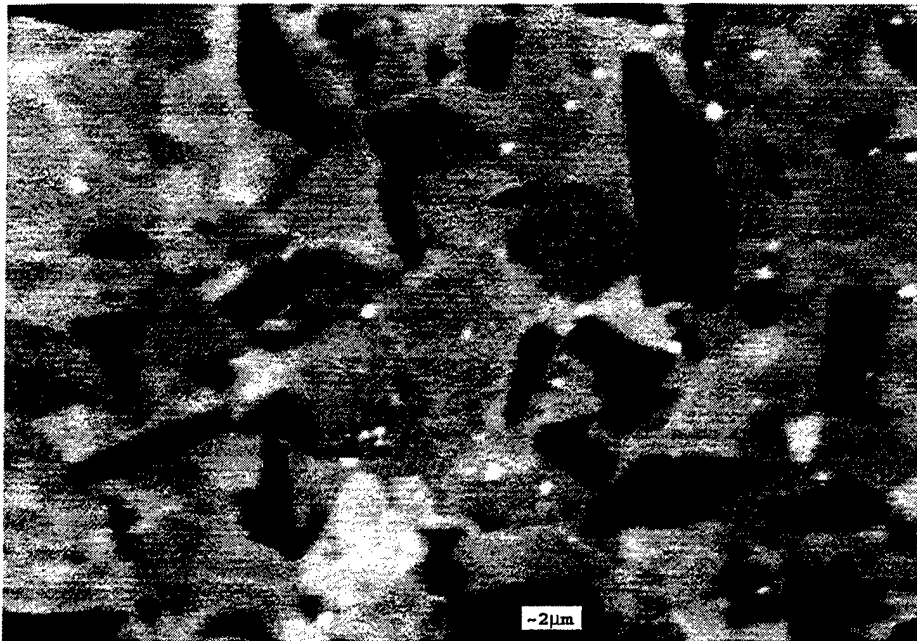


Figure 4.1. Sample 13184, sectioned from normal plane, at 3000x; BSE image at 6kV. This sample had the additional step of chemical polishing with colloidal silica before ion milling. Note what appears to be grain contrast (no etchant).

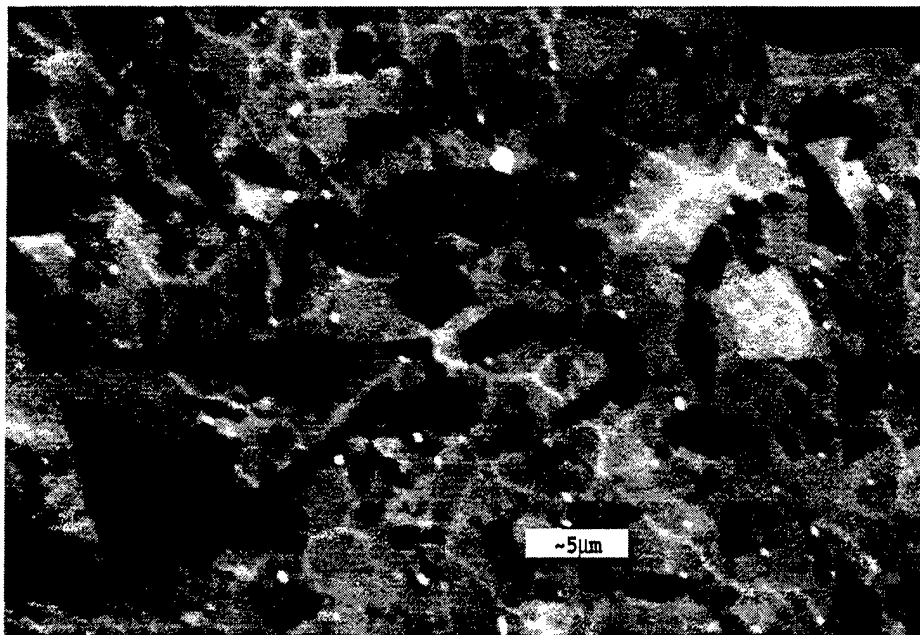


Figure 4.2. Back scatter image at 2500x at 6 kV of 13184 sample, normal plane, with W source. Note what appears to be orientation contrast (no etchant).

B. MICROTEXTURE AND MISORIENTATION ANALYSIS

Approximately 300 electron backscatter patterns were obtained for each of the four samples. The resulting microtexture and misorientation analyses are summarized in Figures 4.3-4.8. The data are in the form of discrete pole figures and, separately, misorientation angle histograms. For all four processing conditions the texture is essentially random; any tendency toward preferred orientation is very weak. Within the limitations of ~300 misorientations, the data are very close to a random distribution (Mackenzie random for cubes [Ref. 22]). Sample 13186 was analyzed with an additional 100 extra data points and no appreciable difference is noted in the data for this processing condition. During collection of the MDP data on this sample, the location of the SiC particles was logged. The APR software allows for misorientation data to be calculated for all successive grain boundaries (i.e. 1-2,2-3,...) or by pairs of orientations (1-2,3-4,...). The data file was edited to eliminate odd numbers of points so that no misorientation measurements were made across any known SiC particle. This procedure allows examination of Al-Al boundaries only, where the grains share a boundary, i.e. there is no intervening SiC particle. Comparing of the misorientation plots in Figures 4.5 and 4.6 indicated essentially no difference between the two results. It would seem that the effect of measuring misorientations across the particles adds some variability to the distribution data but does not add any artifacts.

The microtexture and grain boundary misorientation data are consistent with the occurrence of recrystallization during and immediately following the straining of the final extrusion operation. The generation and motion of dislocations within the deformation

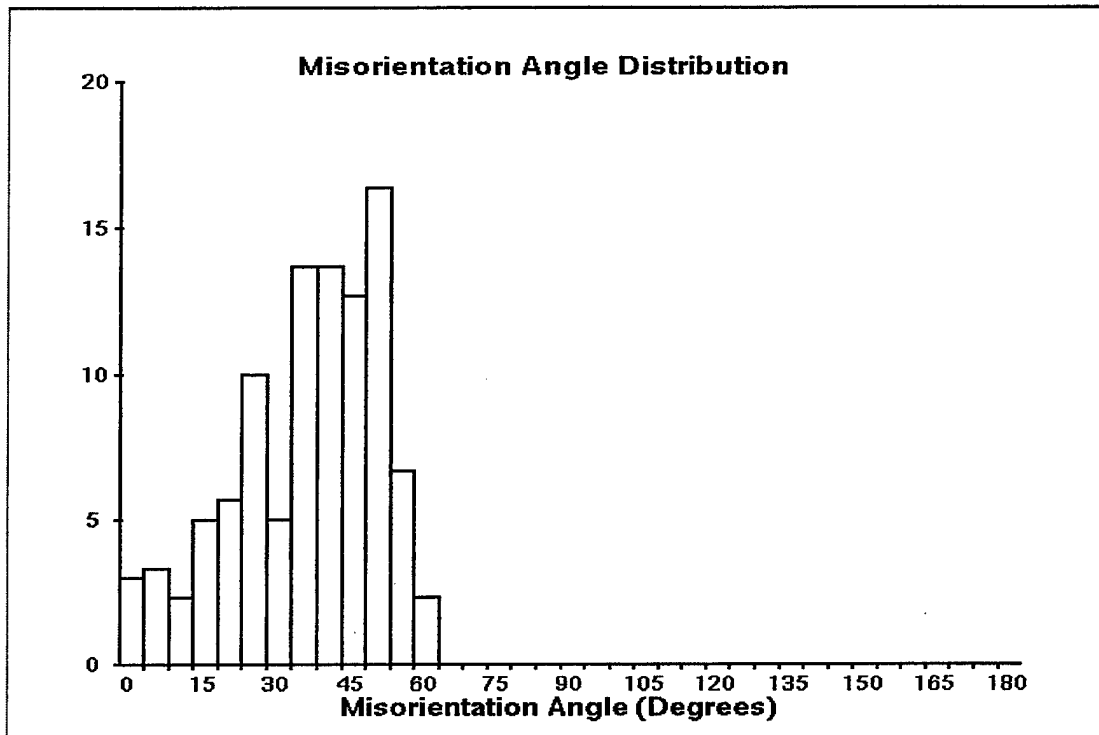
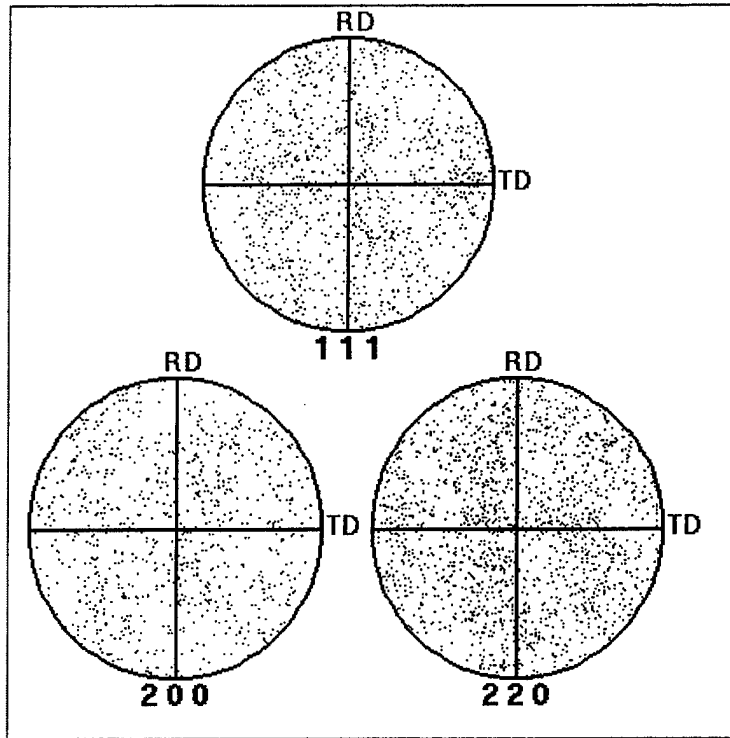


Figure 4.3. Orientation and misorientation data for sample 13183.

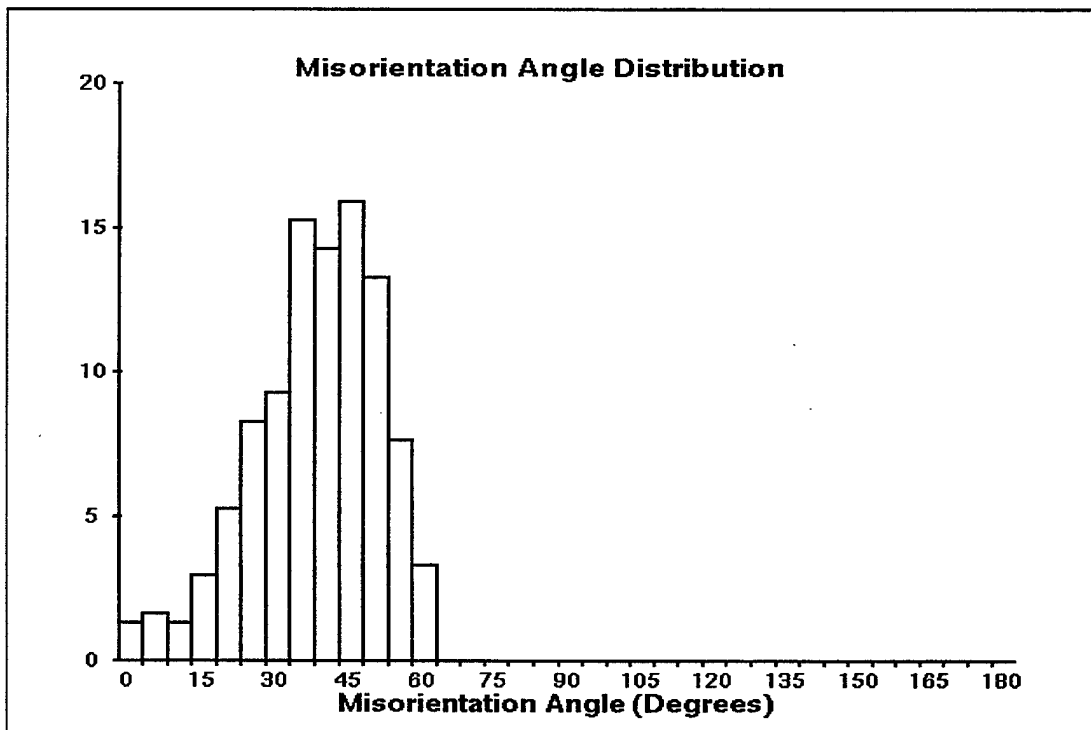
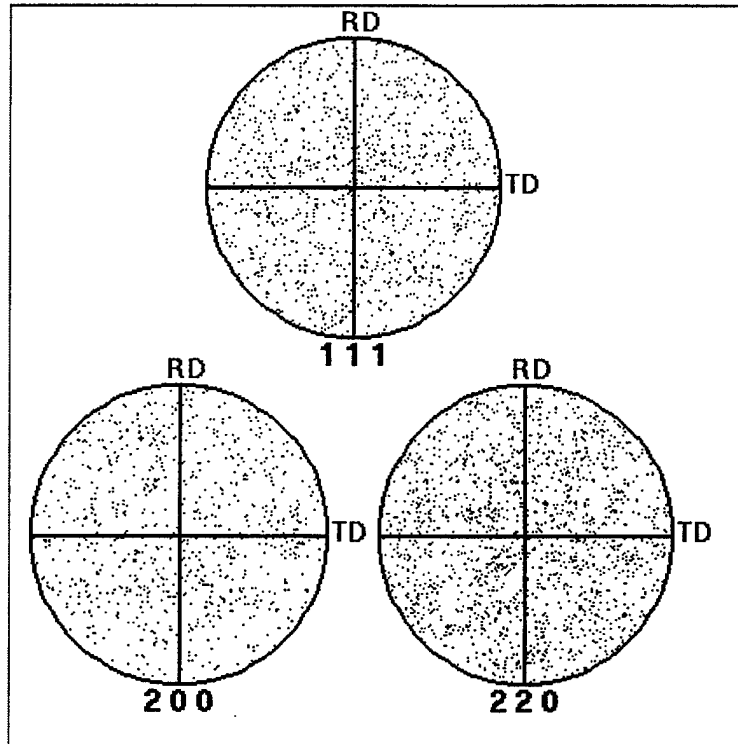


Figure 4.4. Orientation and misorientation data for sample 13185.

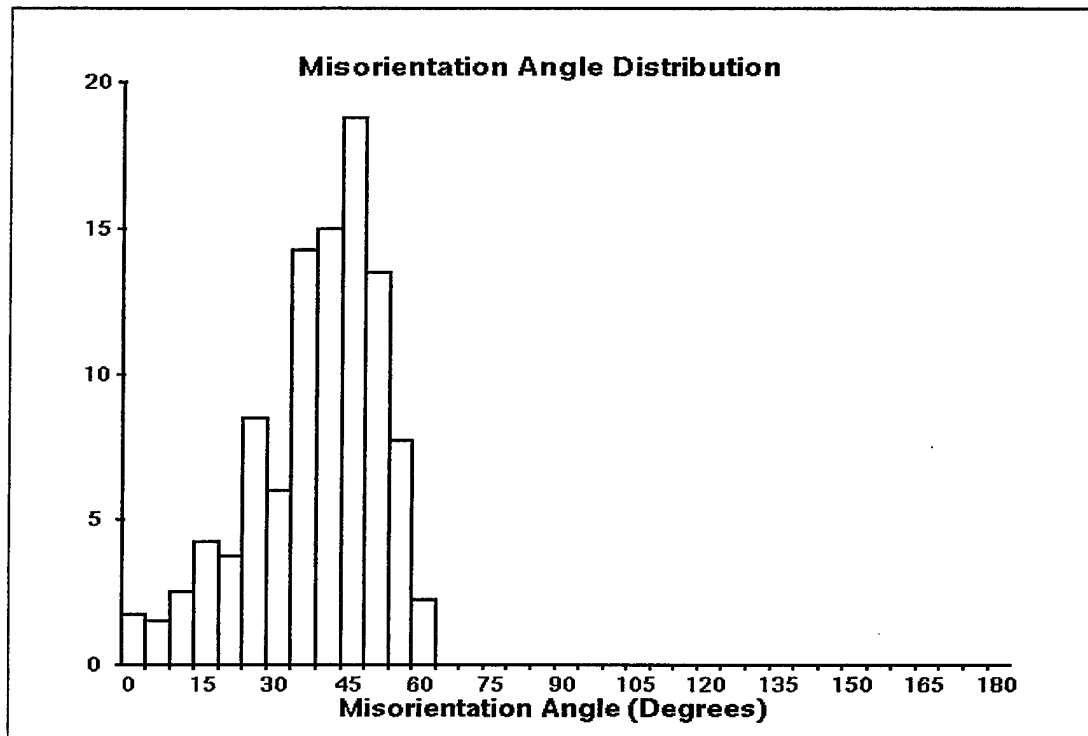
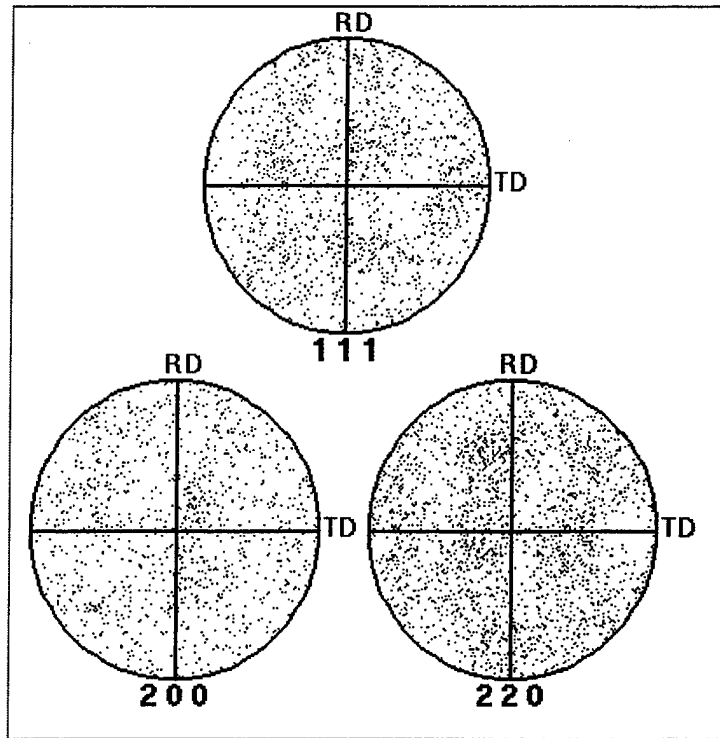


Figure 4.5. Orientation and misorientation data for sample 13186.

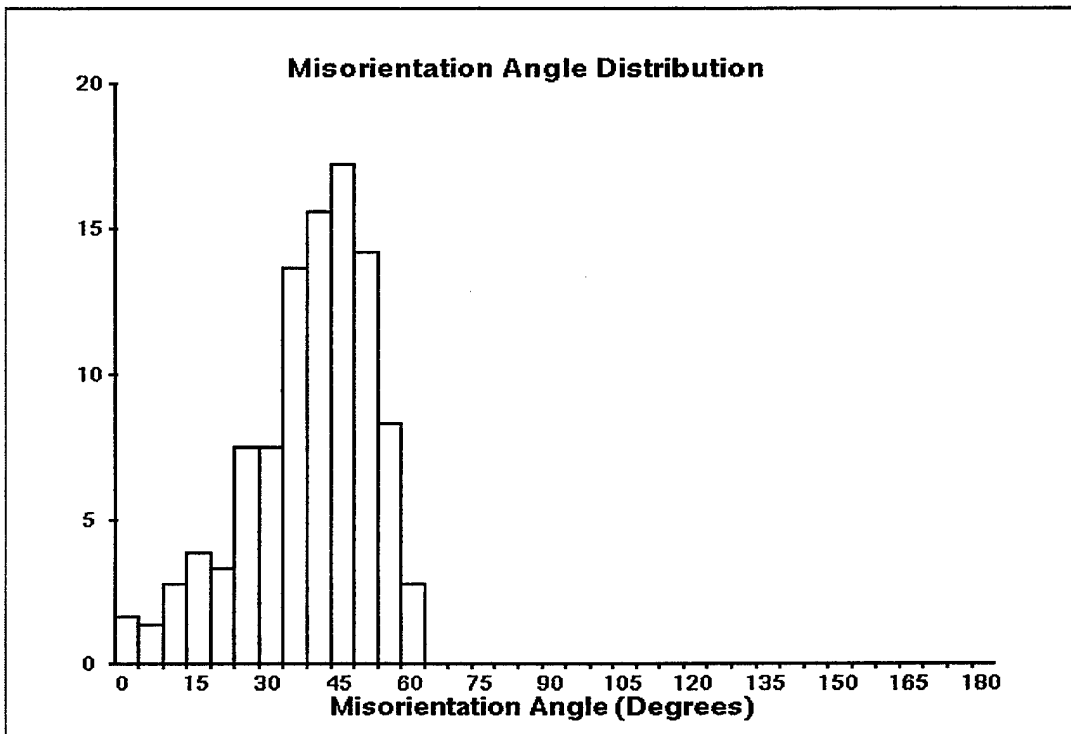


Figure 4.6. Misorientation data for sample 13186, measured for pairs of Al patterns only.

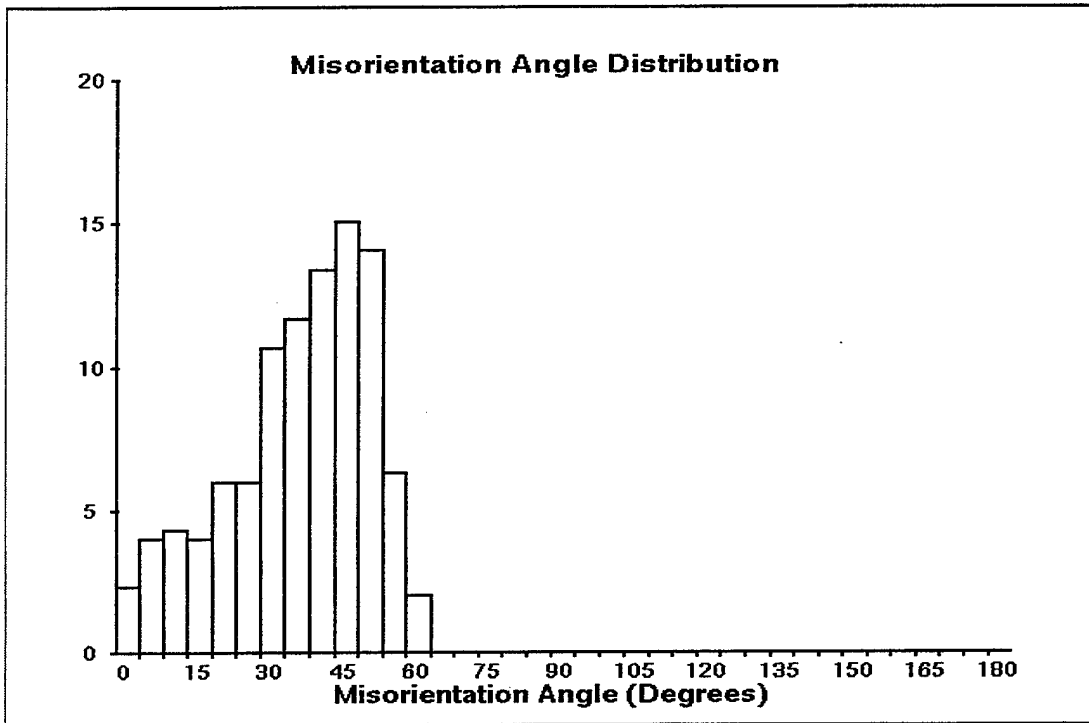
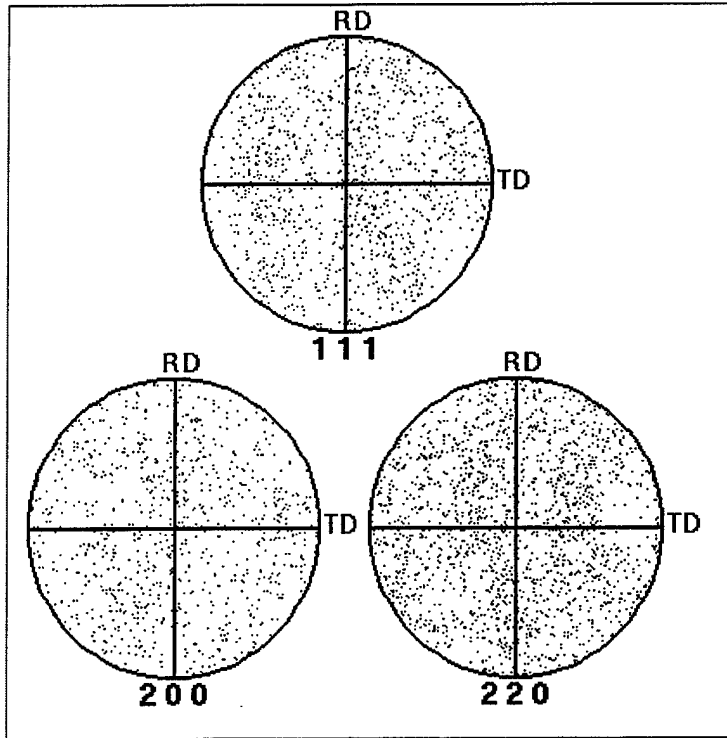


Figure 4.7. Orientation and misorientation data for sample 13187.

zones surrounding the SiC particles will tend to occur in a manner so as to maintain compatibility across the particle/matrix interfaces in the material. Thus, it is expected that lattice rotations in these regions will be random in nature, leading to random orientations for recrystallization nuclei. Equation (2) from the PSN model predicts this for three of the four conditions examined. However, 13187 was extruded at a temperature $\sim 100^{\circ}\text{C}$ above the critical temperature for the strain rate employed in processing. Despite this, the data are consistent with recrystallization for this condition as well.

C. MEAN DISTANCE BETWEEN PATTERNS

Recording of the distance traversed between successive orientation measurements resulted in data which may be treated in the same fashion as mean linear intercept measurements in grain size determination. The individual measurements for each sample are provided in the Appendices B through F. In each case, the data were plotted in the form of histograms using 10 bins of equal spacing range. This number of bins is somewhat higher than the number suggested by the relationship

$$k = 1 + 2.2 \log(n) \quad (6)$$

where k is the number of bins and n is the number of measurements [Ref. 23]. For ~ 300 spacing measurements, $k \cong 6$. In each case, the bin classification was converted into a spacing value (in μm) and the histograms were replotted as shown in Figure 4.8. The resulting peak height versus spacing data were evaluated using the statistical analysis functions in Sigma Plot. In all cases, the best data fits were obtained with a three parameter log-normal distribution function of the form:

$$f = a \exp \left\{ -\frac{1}{2} \left(\frac{\ln \frac{x}{x_0}}{b} \right)^2 \right\} \quad (7)$$

where a is a constant, b is the variance, x_0 is the mean, and x is the pattern-to-pattern spacing. The curve fits and corresponding fitting parameters are included in Figure 4.8.

The log-normal distribution is asymmetrical so the mean values, x_0 , are less than the arithmetic means of each set of the data. The mean values and corresponding 99% confidence intervals are plotted in Figure 4.9. The data are plotted versus a temperature-compensated deformation rate (i.e. a Zener parameter), $\dot{\epsilon} \exp\left(\frac{Q_{SD}}{RT}\right)$, where $\dot{\epsilon}$ is the extrusion strain rate, T is the absolute temperature, and $Q_{SD} = 141 \text{ kJ mol}^{-1}$ is the activation energy for self diffusion in Al. These data clearly suggest that processing results in a fine and constant recrystallized grain size for the range of conditions investigated.

D. UNREINFORCED 6061

A control sample from a bar of 6061T6 Al was analyzed and the orientation and misorientation data shown in Figure 4.10 were obtained. This material exhibits a weak fiber texture, with [100] parallel to the fiber axis. It is likely this texture resulted from recrystallization upon solution treatment (normally conducted at about 560°C). Prior rolling deformation would provide the lattice reorientation and stored energy for this.

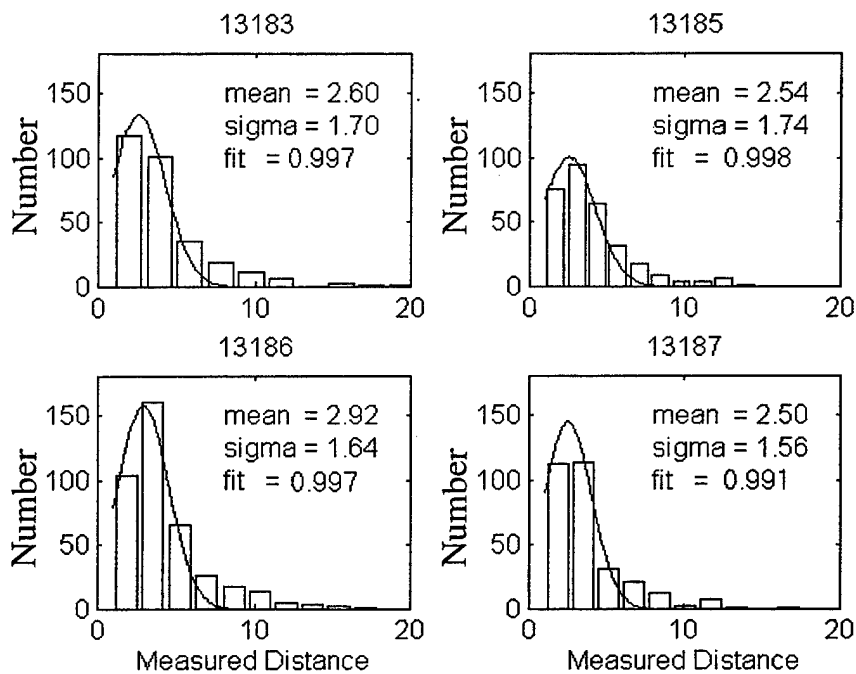


Figure 4.8. Distribution of diffraction pattern distances with log-normal curve fit.

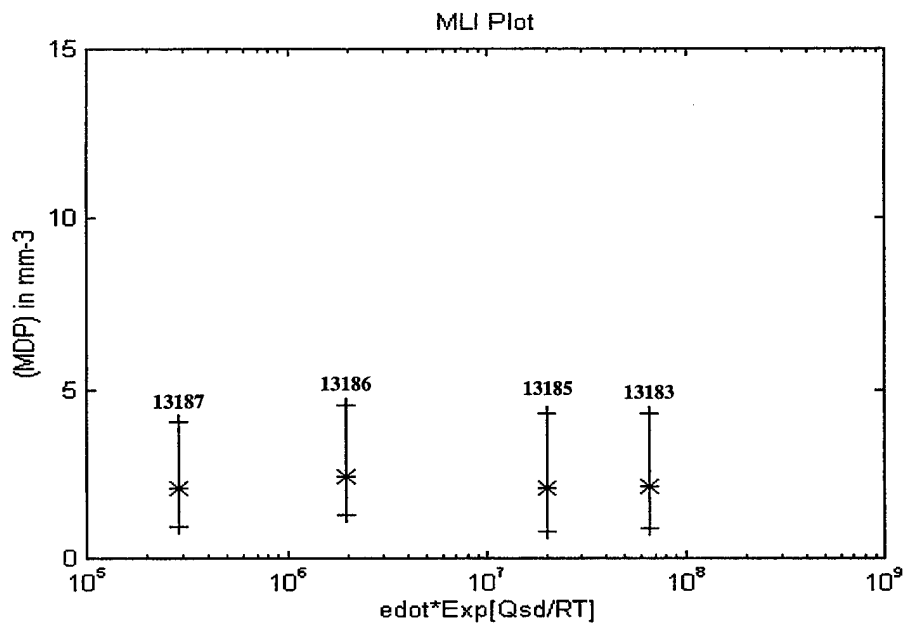


Figure 4.9. Plot of MDP with ± 1 standard deviation as error bracket.

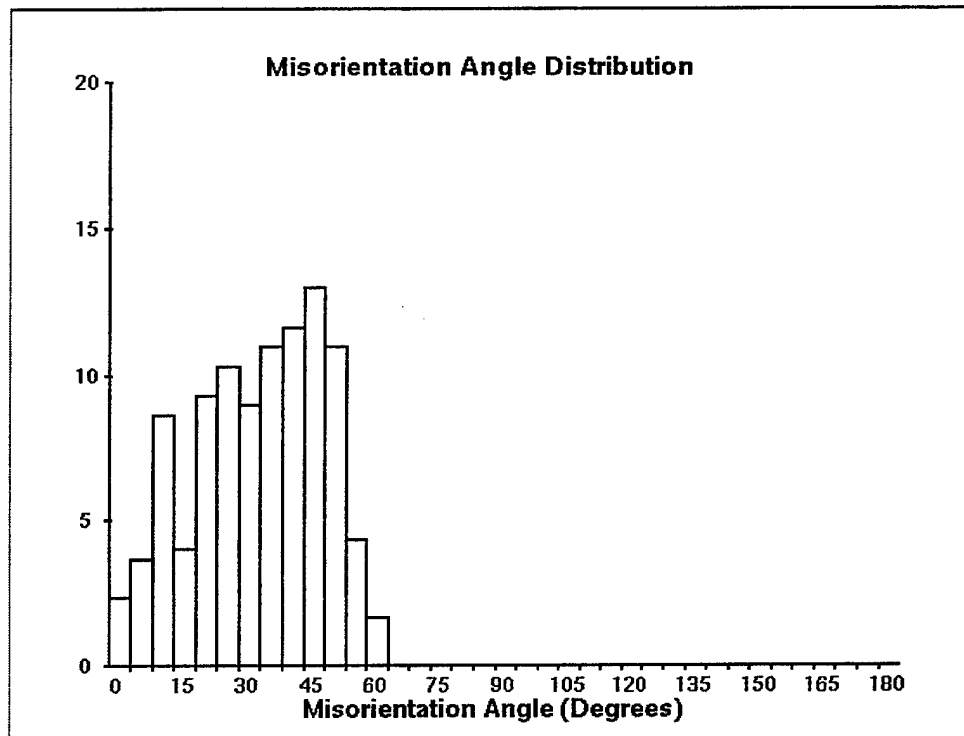
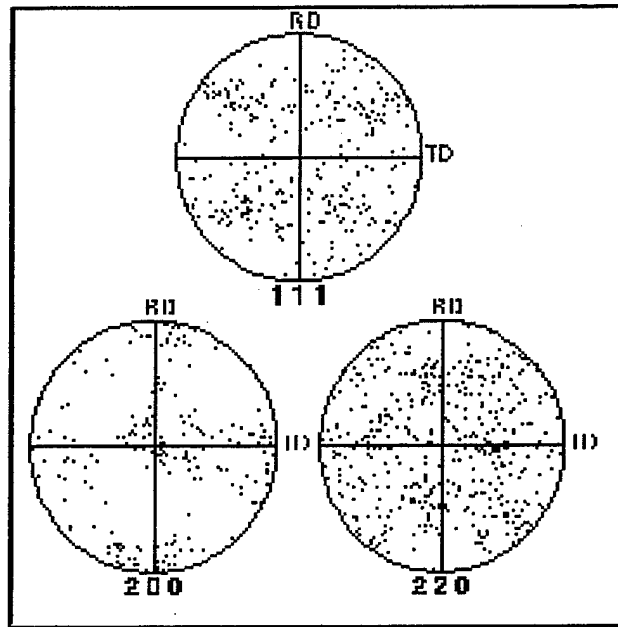


Figure 4.10. Orientation and misorientation data from 6061T6 Al control sample.

With 300 data points, the weak [100] fiber texture is indicated by the concentration of points at the top and bottom of the {200} pole figure and the corresponding bands in the {111} figure. The misorientation data shows a preponderance of high-angle boundaries, but there is also an increase in the number of low-angle boundaries when compared to the more random distributions of the composite.

Finally, the pattern spacing data (Figure 4.11) also exhibit a log-normal distribution but with a mean value of about $28\mu\text{m}$. This value is consistent with a grain size of 30- $40\mu\text{m}$, typical for such an Al alloy.

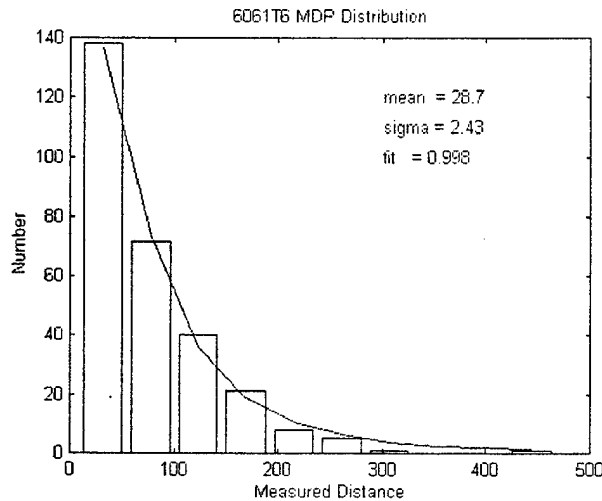


Figure 4.11. Distribution of diffraction distances with log-normal curve fit for 6061T6 rolled Al sample.

V. DISCUSSION

A. COMPOSITE SAMPLE PREPARATION

This research showed that ion milling proved to be adequate in preparing a sufficiently strain free sample to analyze by EBSP methods in spite of the induced roughness. Previous efforts with electropolishing and chemical polishing were not able to reveal matrix grain information. The roughness of the surface causes some concern but does not appear to be a major obstacle in acquiring diffraction patterns.

B. IMPLICATIONS OF THE TEXTURE AND MISORIENTATION DATA

The Humphreys model predicts that three of the four conditions were processed within the PSN regime (Figure 3.1), while one of them was processed well above the critical temperature. The initial analysis employed here relied on the second term for the critical strain rate in Equation (2). The prediction of the model is not improved even if the first term involving lattice diffusion is used instead. The rationale for this would be that the interface diffusivity is much lower in the Al-SiC material because of a higher value of Q_b than reported by Humphreys [Ref. 12] in his work on Al-Si and Al-Ni alloys. When data for lattice diffusion are used, the result illustrated in Figure 5.1 is obtained. Here it is seen that 13183, 13185, and 13186 materials still fall within the PSN regime while 13187 is still well above the critical temperature and therefore not expected to exhibit recrystallization.

PSN Critical Strain Rate (Lattice Diffusion)

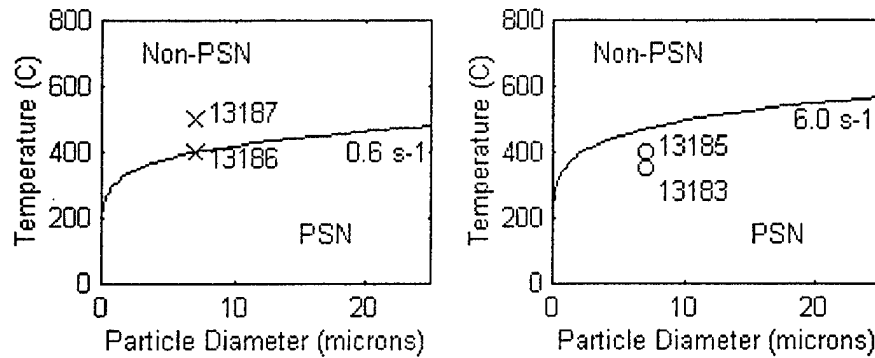


Figure 5.1 Critical processing conditions for PSN with constant strain rate based on the first term in Equation (3).

This suggests that for the critical condition represented by the plots in Figure 5.1 is too low. The presence of the Mg, Si, and Cu alloying additions may retard recovery in this alloy, thus raising the critical temperature for a given processing condition. This effect is not included in the current PSN model and may be needed to reconcile this theory with the current experiment.

C. GRAIN SIZE

The predicted grain size from equation (1) for a composite containing 17.5% SiC particles 7 μm in size is 12.5 μm . This is considerably greater than the size suggested by the MDP analysis of this research. The MDP for 13183 was 2.60 μm . The corresponding grain size is 3.8 μm . This suggests that multiple grains are formed at each particle and that grain growth may be limited. There are, however, several potential sources of error in this MDP measurement.

The first source is operator error. The minimum misorientation that can be measured by this technique is $\sim 1^\circ$. Failure to detect pattern changes corresponding to smaller misorientations would result in an overestimate of the grain size. The operator has to use judgment to distinguish between patterns generated by the matrix and SiC particles. Pattern spacings measured by tracking the traversing knob movement between patterns with a template can also have built in error. The template allowed for measurements of $\pm 0.5\mu\text{m}$; this is 20% of the smallest MDP encountered and is also less than the standard deviation determined by applying a log-normal distribution to the data obtained.

Another possible source of error is from surface roughness incurred from the ion mill. The possible sources of error due to surface roughness are highlighted in Figure 5.1. Data omitted due to overlapping patterns near grain boundaries, data missed completely due to angle of reflection, or due to 'shadowing' by a SiC particle would cause a grain size calculation to be larger than the actual size.

Inadvertantly collecting data from a SiC particle would reduce the MDP. On the 13186 sample, 58 particles were recorded in a total traverse of $1,734.3\mu\text{m}$ while obtaining 400 data points/patterns. For 17.5 % SiC with an average size of $7\mu\text{m}$, there would be just over 43 particles expected to be encountered. The number recorded is of the right order, but if too high, it, too, would cause a calculated grain size to err on the large side.

The consistency of the data collected on all samples and the error analysis, which suggests large errors would make grain measurements appear too large and this suggests that the grain size is indeed less than is anticipated by the Humphreys model. But since

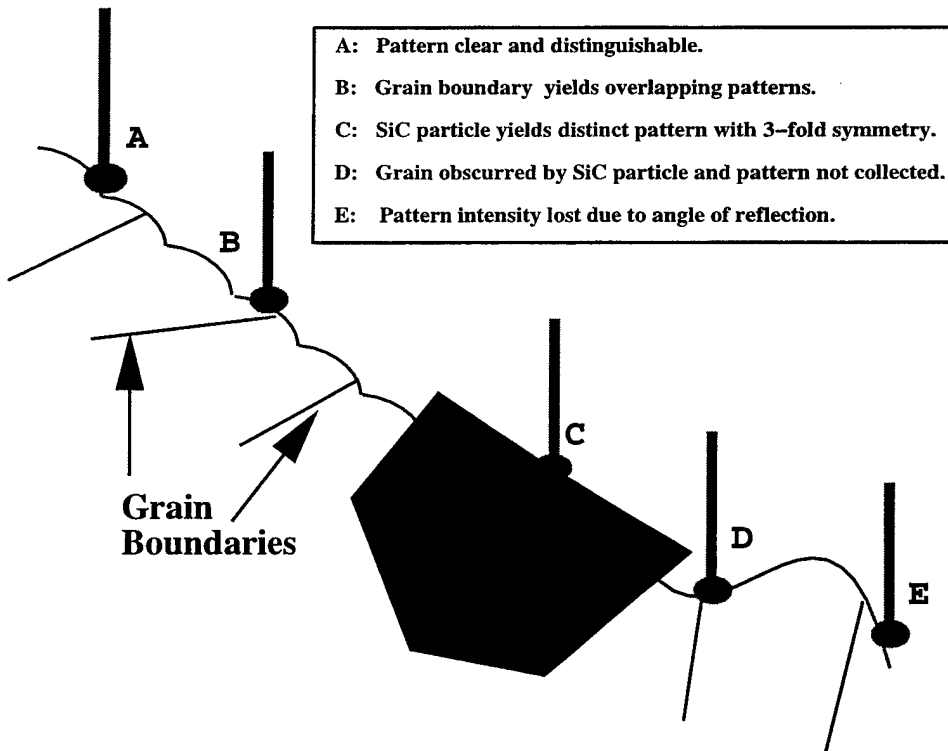
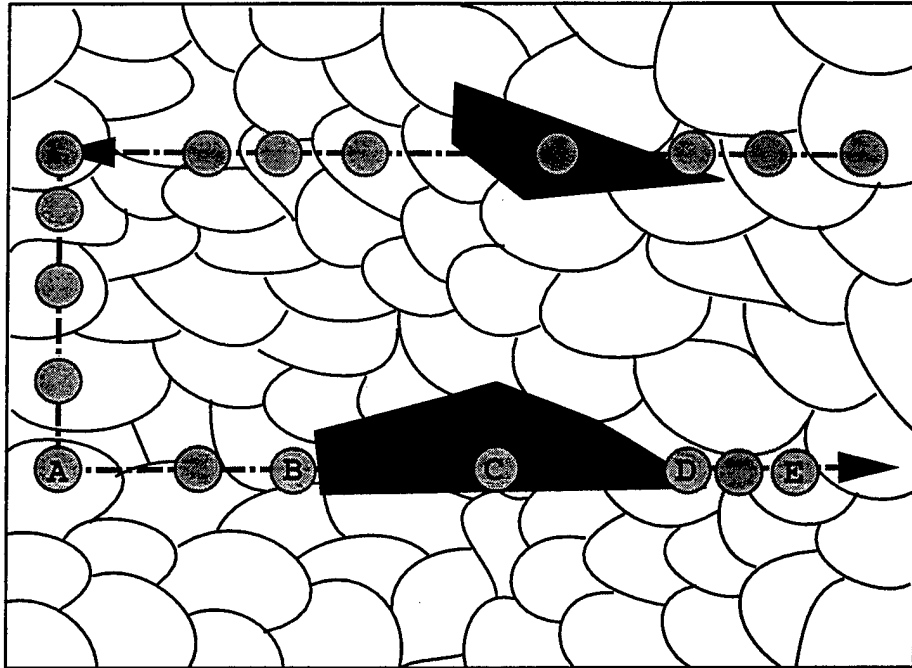


Figure 5.2. Schematic of surface roughness effect on collecting EBSP data while traversing rastering the spot pattern.

such errors remain to be quantified, more refinement of this technique is required before accepting these measurements as actual grain sizes.

An alternative approach to describe grain refinement during processing is a simple geometric model based on the extent of strain applied. The original Al alloy powder particles are 30-50 μm in size. Assuming a cubic shape where the edge $l_0 = 40\mu\text{m}$, and a total strain of 5.67 and using

$$\varepsilon = \ln \frac{A_o}{A} = \ln \frac{l}{l_o}, \quad (8)$$

the result $l = 11,600\mu\text{m}$ is obtained. The area A thus becomes:

$$A = \frac{A_o}{e^{5.67}}, \quad (9)$$

or $A = 5.52\mu\text{m}^2$. The corresponding grain size then becomes 2.35 μm . This is much closer to the mean of the pattern spacing data. Presumably, the elongating grains would be sheared by the particles as they became redistributed. This, however, would likely result in an elongated grain structure, contrary to observation. Also, this geometric model would imply predominance of a slip texture again contrary to observation.

VI. CONCLUSIONS AND RECOMMENDATIONS

A. CONCLUSIONS

From the research described in this report, several conclusions can be drawn:

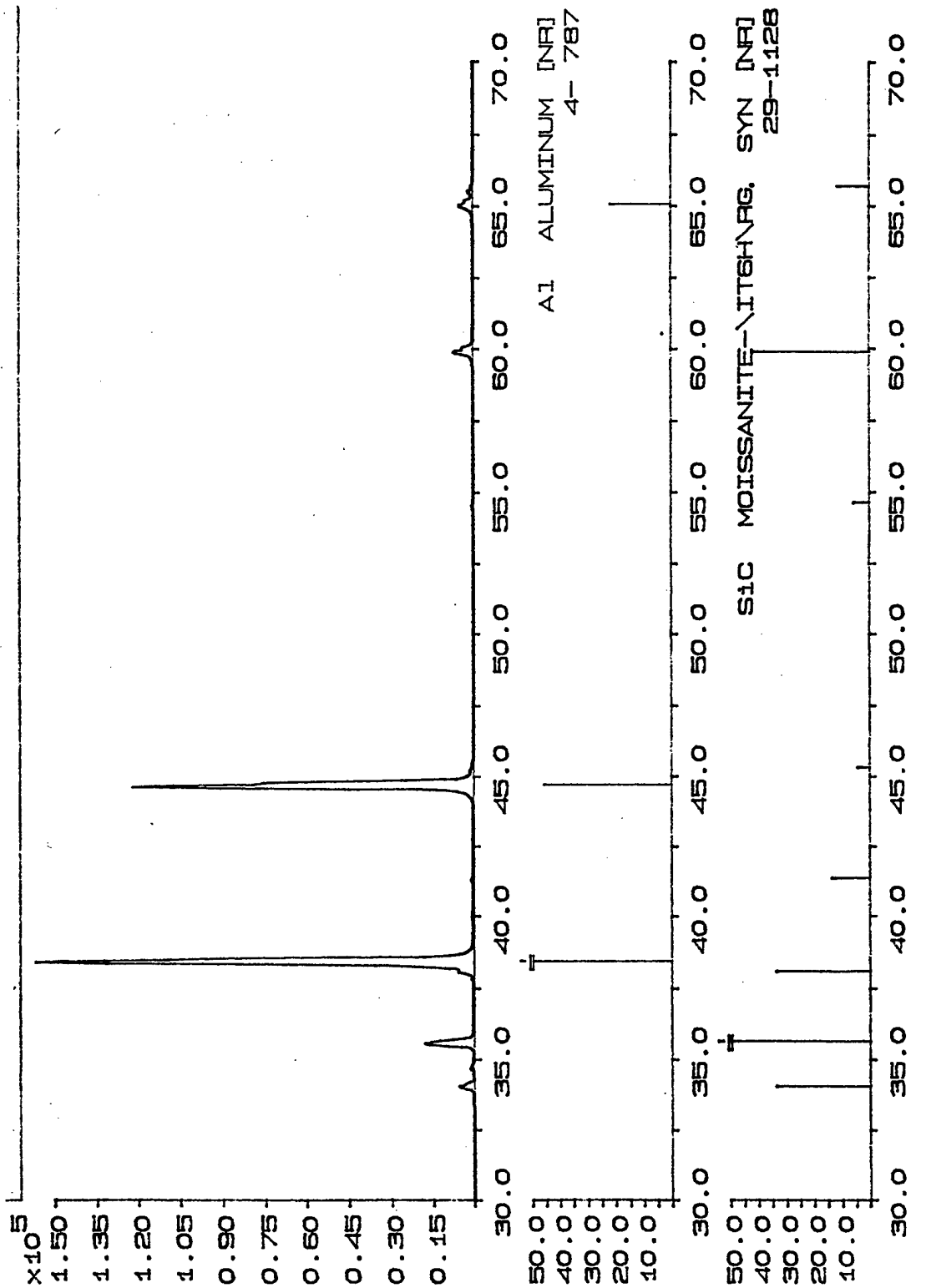
- Successful imaging can be done on the matrix material of an Al-SiC composite material.
- All four processing conditions examined were recrystallized and thus exhibited no texture with random grain boundary misorientation.
- Grain size was finer than expected. It appears that fracture toughness in this composite material may depend on factors in addition to grain size, as in monolithic alloys.

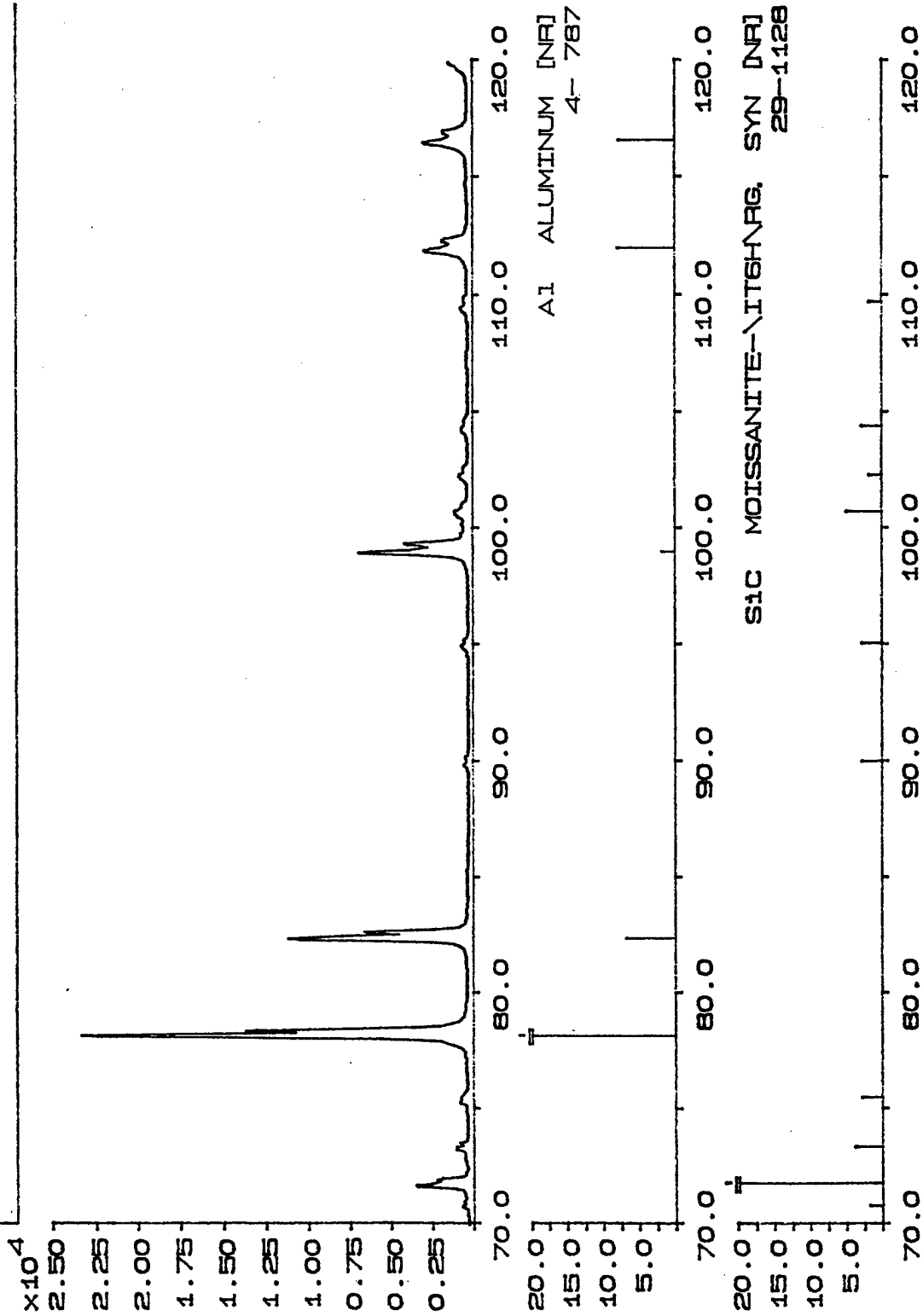
B. RECOMMENDATIONS

In light of this research, several recommendations are made:

- More imaging work needs to be done with this composite material in order to confirm the correlation between MDP and grain size proposed in this experiment. With more refinement, this technique could be used with other particulate composite materials where imaging the matrix grain structure is difficult.
- Other techniques should be used such as XRD to confirm the texture analysis made in this experiment by EBSP methods.
- A control sample of the same 6061T6 Al should be prepared in the ion mill apparatus to ascertain the effect of temperature and roughness effects on the EBSP analysis compared with the sample prepared by electropolishing. This would confirm what role sample preparation had in contributing to the lack of texture seen in the sample processed under non-PSN conditions.

APPENDIX A. XRD ANALYSIS OF 13184





**APPENDIX B. SPACING MEASUREMENTS BETWEEN
ELECTRON BACKSCATTER DIFFRACTION PATTERNS FOR
13183 MATERIAL**

2	2.9	2	2	3	3	3	3
1	5.8	5.8	6	1.5	2	4	1.5
1	3	5.8	2.9	5.8	10	3	2
2	11	2.9	8.8	2.9	3	5	20.4
4	5	4	4	2.9	6	2	3
7	8	3	2.5	2	2	4	4
1	7	1	4	1	17	2	2
2	9	4	6	4	1	7	1
5	2.9	8	2	3	4.4	2.9	3
2	2.9	5	1	7	2.9	2.9	3
4	2.9	2	9	3	2.9	4	3
2	3	3	3.5	2	4	3	5.8
3	3	11	6	1	7	7	2.9
3	2	2	6	2	2	12	2.9
4	3	14.6	2	5	7	2	
2	1.5	2.9	3	7	9	2.9	
1	2	2	2.9	7	2	11.7	
4.4	3	3	2.9	2.9	5	5	
2.9	8	2	5.8	1.5	2	5	
4.4	2	3	2	5.8	2	4	
8.8	4	5	4	2.9	3	2	
2	4	3	5	2.9	2.9	9	
3	2.9	15	5	3	2.9	2	
2.5	8.8	2	5	1	2.9	3	
6	1	1	3	2	4.4	3	
6	7	3	3	4	3	4	
5	2	4.4	2	3	9	2.9	
5	6	4.4	7	3	7	2.9	
1	3	2	1.5	3	9	5.8	
2	5	2	3	2	3	7	
2	4.5	3	2.5	2	1	12	
3	3.5	3	4	8	3	3	
2	3	3	3	3	4	3	
2	2	6	15	2	4	11	
2	2	6	3	3	2.9	5	
2	2	2.5	5	2.9	8.8	3	
3	2	3	3	7.3	4.4	1	
3	4.5	2	3	4.4	4	1	
2.5	3	1.5	4	2.9	8	3	
2.9	3	3.5	2	2	4	3	

**APPENDIX C. SPACING MEASUREMENTS BETWEEN
ELECTRON BACKSCATTER DIFFRACTION PATTERNS FOR
13185 MATERIAL**

3.5	11.7	3	6	1	2.9	2.5	4
3	6	2.5	4	5	2.9	9	1
4	3	1	2.5	2	1	4	1
3.5	9	6	3	2.5	2	6	3.5
2	2	2	3.5	5	1	3	4
7	4	4	3	5	2	5	1
3	6	5	2	4	2	3	5
2	4	2	3	2	7	2.9	4
6.5	7.3	4	8	2	2	2.9	1
3	2.9	6	3	2	3	8.8	2
3.5	2.9	3	4.3	1.5	13	7	3
4	2.9	10	4.3	2	4	5	3.5
2	2	2.9	2.9	2	8.8	9	2
7.3	12	2.9	7	5	5.8	1	2
5.5	5	2.9	7	2.9	4	2	2
2	3.5	2.9	2.5	2.9	2	3	3
6	5	10	4	2.9	5	7	4
9.5	3	7	3	6	4	4	2
5	2	3.5	3	7	3	2.9	2
7.5	2	8.5	3	12	2	5.8	7
13	1	1.5	2.5	3	2	2.9	2
4	5	6	3.5	4	3	2	6
1.5	5	2.9	3	2	3	5.5	5
5.5	7	5.8	2	1	3	2	2
2.9	2	2	2	2	3	1	1
2.9	4	4	1	1	5	2	4
2.5	4	2	5.8	3	2	1	5.8
2.5	12	3.5	2.9	6	5.8	3	
3.5	5.8	5	2	2.9	14.6	4	
4	5.8	2.5	4	2.9	5.8	2	
7	4	4	3	2.9	11	4	
2.5	4	3	7	5	5	2	
7	11	6	11	5	4	3	
2	4	3	2.5	5	10	4	
5	2	12	2	2	8.8	2.5	
2	6	5.8	2.5	5	2.9	4	
2.5	7	5.8	4	9	2.9	5.8	
5	5	2.9	2.9	3	2	5.8	
3	1.5	2.9	4.4	3	2	6	
2.9	1.5	2	5.8	2.9	3.5	2.5	

**APPENDIX D. SPACING MEASUREMENTS BETWEEN
ELECTRON BACKSCATTER DIFFRACTION PATTERNS FOR
13186 MATERIAL(SiC PARTICLE LOCATIONS UNDERSCORED)**

<u>10.5</u>	6.5	<u>2.5</u>	3	4	4	3	7	3	5
6	1.5	<u>9</u>	<u>1.5</u>	4	2.5	5	<u>6.5</u>	3	2.9
4	2.5	13	11.6	2	4	2.9	3.5	4.4	5.8
4	3	3	4	2.5	<u>2</u>	4.4	4	8.8	3
4	4	6.5	2	3	3.5	1.5	3	<u>3.5</u>	3
<u>3</u>	3	2.5	6	1.5	3	1.5	<u>1</u>	12	4
<u>14</u>	<u>5</u>	<u>8</u>	<u>5</u>	4	2	2.9	<u>7.3</u>	3	3
8	2.9	4	6	3	<u>2</u>	4	8.8	3	2
4.4	<u>1.5</u>	3.5	4	4	6	5.5	1.5	2	3
5.8	5.8	<u>2</u>	7.5	2.9	3	3	2.5	5	3
2.9	5	<u>10</u>	<u>1.5</u>	2.9	4.5	7.5	2	6	3.5
<u>4</u>	7.5	13	4	5.8	<u>3</u>	11	2	<u>2.5</u>	1
6	3	1.5	1.5	2.9	7.5	3	5	5	4
<u>2</u>	1.5	2.5	2.9	2	4.5	4.5	<u>5</u>	2	2
10	3	4.5	1.5	5	6	2.9	15	4.4	2
7	11	4	4.4	<u>6</u>	<u>2.9</u>	2.9	7	4.4	2
3.5	4	<u>2.9</u>	<u>4</u>	10	5.8	2.9	2.5	4.4	3.5
1	3.5	11.6	12	18	4.4	8.8	2	4	8.8
4	2	6	2	<u>2.9</u>	1.5	1.5	<u>2.5</u>	4	5.8
4	2	<u>7</u>	4	13.1	4.5	5	5.8	1.5	2
2	2.9	6	3	1.5	<u>3</u>	6.5	5.8	6	8
7	2.9	3.5	5.5	10	6	2	<u>1.5</u>	<u>5</u>	<u>2.5</u>
2.9	2.9	<u>2</u>	3	4	9	<u>4</u>	8	11	9
1.5	2	4	<u>3</u>	2	<u>2</u>	12	1	3	3
2.9	7	4	7.5	3.5	7	1.5	<u>3.5</u>	4	1
3	1	<u>7</u>	2.9	5	3	6	7	3	2
4	3	11	4.4	1	<u>4.4</u>	4.5	2	<u>3</u>	4
<u>3</u>	1	4.4	2.9	1.5	8.8	2	5	7.3	3
<u>9</u>	1.5	2.9	5.8	2.5	2	2.9	2.5	2.9	2
7	<u>5</u>	2.9	<u>3.5</u>	7	5	5.8	<u>1.5</u>	<u>2.9</u>	1.5
2	7.5	2.9	10	3.5	6	1.5	6	7	2.9
5	3	2	<u>2</u>	2.5	2	2.9	4	8	2.9
6	1.5	<u>5</u>	15	5.8	2	3	3	3	2.9
2.9	4	6	3	2.9	7	2.5	<u>3</u>	2.5	<u>1.5</u>
4.4	2	<u>4.5</u>	5.8	1.5	4	3	2	<u>3</u>	8.5
2.9	3	10	4.4	1	5.8	3	11	7	3
1.5	1.5	3	2.9	<u>3.5</u>	5.8	2	2	<u>4</u>	4
5.5	3.8	2.5	4.4	10	<u>6</u>	3	6	3.5	2.5
5	2.9	4	5	3	10.5	6	<u>1.5</u>	1.5	
<u>8</u>	3.5	1.5	3	2	4.5	<u>2.5</u>	9	2	

**APPENDIX E. SPACING MEASUREMENTS BETWEEN
ELECTRON BACKSCATTER DIFFRACTION PATTERNS FOR
13187 MATERIAL**

3	4	7	2	12	3	6	4
5	2	3.5	4.4	10	2	1	2
7	2	1	2.9	6	1	7	4.5
11	1	2	2.9	6	4	2	11
2	1	5	2.9	2.9	5	1.5	3
4	2.5	4	8.8	7.3	4	6	6
4	2	8.8	9	3	4	1	3
3	1	5.8	8	3	2	7	4
4	4	4	3	3	2	2	8.8
2.9	17.5	1.5	7	4	1.5	1.5	7.3
5.8	3	10	2	4	2	2	5
13	6	3.5	4	5	2	2.9	3
1	2.5	9	4	2	4	7.3	5
2	7	3.5	12	1.5	2.8	2.9	4
3	5	2	4	3	5.8	1	3
3	3	2	4	2	2	2	4
3	2	2	1	5	3	2	3
4	3	2	2	3	3	2	4
3	2	4.4	3	3	2	3	1.5
9	8	2.9	3	8	2	5	2
5	8.8	4	2	2	2	4	2
2.9	5.8	4	2.5	1.5	1	1	5.8
2.9	3	2	2.9	1.5	1	3	
4.4	2	2	2.9	2.9	5	1	
1	5	4	2.9	2.9	1	1	
2.5	2	2	4	5	4	3	
2	1.5	1	5	3	8	2	
2	1	4	2	2.5	3	2	
2	2	3	12	2	4	2	
2	2	3	3.5	2	2	2	
2.5	3	2	2	6	2.9	2	
2	3	5	2	1	2.9	1.5	
1	3	5.8	6	10	2.9	1	
2.9	2	8.8	3	2	2	2	
2.9	1	5	2	7	3	1.5	
2.9	2.9	6	3	1	3	2.9	
1.5	2.9	7	4.4	2.9	11	2.9	
12	3.5	7	4.4	2.9	2	5.8	
3	3	4	2	4.4	2.5	7.5	
4	3	4	4	5	1.5	3	

LIST OF REFERENCES

1. Chawla, K.K., *Composite Materials*, Springer-Verlag, New York, 1987.
2. Chin, E.S.C, Beck, J.C., Huang, P.J., Wickman, H.A., Biederman, R.R., "Thermomechanical Processing of Metal Matrix Composites for Ballistic Protection", Proceedings of the Sagamore Army Materials Research Conference, pp. 197-213, 1993.
3. Private communication between Professor Terry R. McNelley of the Naval Postgraduate School and Dr. E.S. Chin of the Army Research Laboratory-Materils Directorate, February 1998.
4. Hoyt, W.F., "The Effect of Thermomechanical Processing on Mechanical Properties of a Cast 6061 Aluminum Metal Matrix Composite", Masters Thesis, Naval Postgraduate School, Monterey, California, December, 1993.
5. Ballou, Michael A., "The Effect of Thermomechanical Processing on the Tensile Properties and Microstructure of a Cast 6061 Al-Al₂O₃ Metal Matrix Composite", Masters Thesis, Naval Postgraduate School, Monterey, California, December, 1995.
6. Dutta I., Quiles F.N., McNelley T.R., and Nagarajan R., "Optimization of the Strength-Fracture Toughness Relation in Particulate Reinforced Aluminum Composites via Control of Matrix Microstructure", *Metalurgical and Materials Transactions*, in publication.
7. Longnecker, F.W., "An Analysis of the Microstructure and Reinforcement Distribution of an Extruded Particle-Reinforced Al 6061-10 Volume Percent Al₂O₃ Metal Matrix Composite", Masters Thesis, Naval Postgraduate School, Monterey, California, September 1993.
8. Kalu, P.N. and McNelley, T.R., "Microstructural Refinement by Thermomechanical Treatment of a cast and Extruded 6061 Al-Al₂O₃ Composite", *Scripta Metallurgica et Materialia*, Vol. 25, pp. 853-858, 1991.
9. McNelley, T.R. and Kalu, P.N., "The effects of Thermomechanical Processing on the Ambient Temperature Properties and Aging Response of a 6061 Al-Al₂O₃ Composite", *Scripta Metallurgica et Materialia*, Vol. 25, pp. 1041-1046, 1991.
10. McNelley, T.R., Ballou, M.A., Dutta, I., "A Microstructural Investigation of Particle Redistribution During TMP of a Cast 6061 Al-Al₂O₃ MMC", *Processing, Properties and Applications of Cast Metal Matrix Composites*, The Minerals, Metals, & Materials Society, 1996.
11. Humphreys, F.J., "The Nucleation of Recrystallization at Second Phase Particles in Deformed Aluminum", *Acta Metallurgica*, Vol. 45, pp. 1323-1344, 1977.

12. Humphreys, F.J., Kalu, P.N., "Dislocation-Particle interactions During High Temperature Deformation of Two-Phase Aluminum Alloys; *Acta Metalurgica*, Vol. 35, pp. 2815, 1987.
13. McNelley, T.R., Crooks, R., Kalu, P.N., Rogers, S.A., "Precipitation and Recrystallization During Processing of a Superplastic Al-10Mg-0.1Zr Alloy", *Material Science & Engineering*, A166, pp.135-143, 1993.
14. McNelley, T.R., McMahon, M.E., "Recrystallization and Superplasticity in Aluminum Alloys", *Superplasticity and Superplastic forming*, A.K. Ghosh and T.R. Bider (eds.), pp.75-87, 1998.
15. Quiles, F.N., "An investigation of the Effects of Secondary Processing on the Fracture Properties of a SiCp-6XXX Al Composite", Masters Thesis, Naval Postgraduate School, Monterey, California, June, 1996.
16. Williams, David B. and Carter, C. Barry, *Transmission Electron Microscopy: a Textbook for Materials Science; Basics: Volume I*, Plenum Press, pp. 162-165, 1996.
17. Course Literature, Orientation Imaging Academy, TexSem Laboratories Inc., Provo, Utah, 1998.
18. Course Literature, Orientation Imaging Academy, TexSem Laboratories Inc., Provo, Utah, 1995.
19. McMahon, M.E., "Grain Bondary Development in Superplastic Aluminum", PhD. Dissertation, Naval Postgraduate School, Monterey, California, December, 1996.
20. Metals Handbook, Tenth edition, Vol. 9, edited by Joseph R. Davis et al.; ASM International, pp.129-134, 1990.
21. Barret, Charles F., *Structure of Metals: Crystallographic Methods, Principles, and Data*, McGraw-Hill, New York, pp. 442-509, 1952.
22. MacKenzie, J.K., "Second Paper on Statistics Associated with the Random Disorientation of Cubes", *Biometrika*, Vol.45, pp. 229-240, 1958.
23. Larson, Harold J., *Statistics: An Introduction*, Krieger Pulishing Company, Malabar, Florida, p.15, 1983.
24. Mcnelley, T.R., Ballou, M.A., and Dutta, I., "A Microstructural Investigation of Particle Redistribution During Thermomechanical Processing of a Cast 6061 Al-Al₂O₃

MMC", Processing, Properties and Applications, Edited by P.K. Rohatgi, pp. 143-153 , 1996.

25. McQueen, H.J., Xia, X., and Myshlyaev, M., "Dynamic Recrystallization in Hot Working of Aluminum Alloy Matrix Particulate Composites", Proceedings of ReX'96, The Third International Conference on Recrystallization and Related Phenomena, pp. 603-610, 1997.

26. Kaibyshev, R. and Kazyhanov, V., "Mechanism of Static Recrystallization in Severely Strained Metal Matrix Composite", Proceedings of ReX'96, The Third International Conference on Recrystallization and Related Phenomena, pp. 619-626, 1997.

27. Mabuchi, Mamoru and Higashi, Kenji, "Grain Size Control in Metal Matrix Composites", Proceedings of ReX'96, The Third International Conference on Recrystallization and Related Phenomena, pp. 611-618, 1997.

28. Miller, W.S. and Humphreys, F.J., "Strengthening Mechanisms in Particulate Metal Matrix Composites", Scripta Metallurgica et Materialia, Vol. 25, pp. 33-38, 1991.

29. Miller, W.S. and Humphreys, F.J., "Strengthening Mechanisms in Particulate Metal Matrix Composites", Scripta Metallurgica et Materialia, Vol. 25, pp. 33-38, 1991.

30. Loretto, M.H., Electron Beam Analysis of Materials, Chapman and Hall, London, 1984.

31. Callister Jr., W. D., *Materials Science and Engineering: An Introduction*, John Wiley & Sons, New York, pp. 169-173, 1994.

32. Cullity, B.D., *Elements of X-Ray Diffraction*, 2nd Ed., Addison Wesley, pp. 480-496, 1978.

33. Newbury, Dale E., Joy, David C., Echlin, Patrick, Fiori, Charles E., and Goldstein, Joseph I., *Advanced Scanning Electron Microscopy and X-Ray Microanalysis*, Plenum Press, New York, pp. 99-107, 1987.

INITIAL DISTRIBUTION LIST

1. Defense Technical Information Center.....2
8725 John J. Kingman Rd., STE 0944
Ft. Belvoir, Virginia 22060-6218
2. Dudley Knox Library.....2
Naval Postgraduate School
411 Dyer Rd.
Monterey, California 93943-5101
3. Naval Engineering, Code 34.....1
Naval Postgraduate School
Monterey, California 93943-5100
4. Department Chairman, Code ME/Mc.....1
Department of Mechanical Engineering
Naval Postgraduate School
Monterey, California 93943-5000
5. Professor Terry R. McNelley, Code ME/Mc.....1
Department of Mechanical Engineering
Naval Postgraduate School
Monterey, California 93943-5000
6. Dr. Wilbur Simmons.....1
Material Science Division
U.S. Army Research Office
P.O. Box 12211
Research Triangle Park
North Carolina, 27709-2211
7. Dr. Ernest Chin.....1
Army Research Lab
AMRSL-MA-MR
APG, Maryland, 21005-5069
8. Dr. Dan Miracle.....1
Wright Laboratory
WL/MLLM
WPAFB, Ohio, 45433

9. Dr. Don Lesuer.....1
Lawrence Livermore National Laboratory
P.O. Box 808
Livermore, California, 94550
10. Prof. J. Spicer.....1
102 Maryland Hall
3400 N. Charles St.
Baltimore, Maryland, 21218-2689
11. Mr. Mark van den Bergh.....1
DWA Composite Specialties
21130 Superior St.
Chatsworth, California, 91311-4393
12. MAJ John Markovich, USA.....2
1458 Brenthaven Lane
Florissant, Missouri, 63031